Part I **Structural and dynamic characterization**

Norbert Kučerka, Daniela Uhríková

1 Biophysical perspectives of lipid membranes through the optics of neutron and X-ray scattering

Abstract: Throughout the biological world, cell membranes are crucial to life, with lipids being one of their major components. Although the basic notion of the fluid mosaic model still holds true, the plasma membrane has been shown to be considerably more complex, especially with regard to the diversity and function of lipids. Besides proteins playing an active role in carrying out the various functions that take place in a biological membrane, much attention has recently focused on the importance of lipids in membrane function. After all, how better to explain the diversity of lipids found in nature? Biological membrane mimetics, such as liposomes, lipid bilayers, and model membranes, are used in a broad range of scientific and technological applications due to the unique physical properties of these supramolecular aggregates of amphiphilic molecules. They serve as platforms for studying the soft matter physics of membranes and membrane dynamics, interactions of bilayers with drugs or biologically important molecules like DNA or peptides, and effects of various additives or environmental changes. The modern state-of-the-art research takes advantage of joining brilliance of X-ray scattering sources with some peculiar properties of neutrons and combines results with the power of computer simulations. The advances in chemistry, and deuteration possibilities in particular, allow for better experimental spatial resolution and possibility to pinpoint labels within membranes. It is only a matter of time for many biological functions that occur at the membrane interface to be matched with the structural properties of these membranes. Several examples of pursuing correlations between the structural results of model biomembrane and functions taking place therein will be discussed.

Keywords: biological membrane, lipid bilayer, cholesterol, alcohols, metal ions, DNA, neutron and X-ray scattering

Norbert Kučerka, Department of Physical Chemistry of Drugs, Faculty of Pharmacy, Comenius University in Bratislava, Bratislava, Slovakia; Frank Laboratory of Neutron Physics, Joint Institute for Nuclear Research, Dubna – Moscow Region, Russia
Daniela Uhríková, Department of Physical Chemistry of Drugs, Faculty of Pharmacy, Comenius University in Bratislava, Bratislava, Slovakia

https://doi.org/10.1515/9783110544657-001

1.1 Biological membranes

Biological membrane is a main building block in living organism, where it plays a crucial role in encompassing and defining cells and biological tissue. Membranes form a natural hydrophobic barrier that separates the cytosol from the extracellular environment. However, these complex mesoscopic assemblies have been shown repeatedly to be far more elaborate than simple double-layered structures [1] that serve as permeability barriers [2]. Although the fluid mosaic model [3] remains a dominant theme in our understanding of biomembranes [4], it has evolved to include the notions of a crowding [5] and rafts [6] and turned membranes into highly functional dynamic machines that are central to a host of biological processes, including the transport of materials, cell defense, recognition, adhesion, and signaling [7]. Consequently, as structure is often tightly coupled to function, the myriad-specific functions occurring in these membranes are plausibly correlated with the lipidome's size and diversity [8].

Biological membranes consist mainly of lipids and proteins, where it is widely accepted that the membrane's underlying structure is imparted by the lipid bilayer. Due to the compositional complexity of biological membranes, the physical properties and functional roles of individual lipid species are exceedingly difficult to determine. In order to gain insight into the roles of individual components, it is necessary to study model membrane systems that contain the lipid species of interest. For example, in eukaryotic cells, the predominant lipid species are glycerol-based phospholipids, including phosphatidylcholine (PC), phosphatidylethanolamine (PE), phosphatidylserine, phosphatidylglycerol (PG), phosphatidylinositol, and cardiolipin (CL), while major phospholipids observed in prokaryotic membranes constitute PE, PG, and CL [9]. Furthermore to the headgroup diversity, each lipid species exhibits although characteristic yet fairly diverse fatty acid composition.

It is well known that lipid bilayers form spontaneously due to the hydrophobic effect [10], whereby their structure is dictated by the fine balance of the forces that minimize the system's total free energy. This includes both entropic and enthalpic components that are related to the disruption of the hydrogen bonding network between water molecules, van der Waals attractive forces, *trans*-gauche isomerization, and, most likely, other interactions [11,12]. Changes to hydrocarbon chains can affect all the mentioned intrabilayer interactions, resulting in different equilibrium structures. It is thus not surprising that lipids with different length hydrocarbon chains and degree of unsaturation were found to form bilayers with different thicknesses and lateral areas at the bilayer–water interface [13]. The mishap in maintaining the fine balance of membrane unsaturation can then again result in disorder and malfunction, as has been recognized recently in gestational diabetes mellitus [14]. Because the cell membrane is a first line of defense against invading species, it is key to understanding various diseases and pharmaceutical treatments. Small molecules, such as cholesterol, melatonin, vitamins, peptides, and many others, incorporate

into the lipid matrix altering the membrane's structure and physical properties. These changes to the membrane in turn affect its functionality and its interactions with biomolecules, while the mechanism of action is often elusive.

There are many experimental techniques suitable for studying biomembranes at the microscopic level. Scattering techniques, on the other hand, have traditionally been used to determine the structure of 3D crystals on atomic levels. However, advances achieved over past decades developed to an extent that scattering approaches can successfully characterize the physical properties of disordered materials such as biomimetic membranes. The X-ray and neutron scattering methods are now applied to elucidate the material properties previously thought to be the domain of other techniques and even provide possibilities not present in any other methods.

Neutron and X-ray scattering are similar in that both techniques are capable of providing dynamical and structural information [15]. However, the principal differences between the two techniques are in their interactions with matter. As X-rays are electromagnetic waves that primarily interact with electrons, the amplitude of X-ray scattering increases in a simple way with atomic number. On the other hand, neutrons are elementary particles that interact with atomic nuclei, and neutron scattering amplitudes depend in a complex manner on the mass, spin, and energy levels of nuclei. Additionally, differences in the interaction of neutrons with the various isotopes of the same element allow for the powerful and commonly used method of contrast variation. This technique, in which hydrogen atoms that are ubiquitous in biologically relevant samples are substituted with deuterium atoms, is commonly used in neutron scattering studies. Neutron diffraction can then determine the distribution of water or individual components through deuterium labeling. The ability to isolate individual molecular groups at atomic level of detail is unique among biophysical techniques, as it does not require model fitting or other interpretation of the data. Furthermore, discovery of the center of mass distribution of a chemical group is information directly comparable to molecular model simulations without the need for additional computations [16]. The recent advances in X-ray and neutron scattering methods in general are increasingly providing us with a unique access to the much-touted structure–function relationship in biomembranes that is universally sought out in biology and pharmacology.

1.2 Structural significance of lipid diversity

Advances in colloid and interface science have stimulated a renewed interest in the study of lipid–water systems. At the same time, much progress has been made in the analysis of small-angle X-ray (SAXS) and neutron scattering (SANS) data [17]. The popularity of small-angle scattering for the study of biologically relevant materials stems from the fact that it provides detailed information on the size, shape, and conformation of molecular

assemblies in solution. As a result, structural biophysics has taken advantage of recent developments to accurately determine the structure of lipid bilayers. An example of this is the joint refinement of X-ray and neutron scattering data [18], which has been rethought in terms of improving the values of lipid areas [19].

The models of X-ray scattering length density (XSLD) and neutron scattering length density (NSLD) emphasize different, but complementary features of the bilayer [13] (e.g., compare Figure 1.1a and b). It follows that a combined approach describes the structural features accentuated by each technique, but in a manner that the data are analyzed simultaneously. This is illustrated in the way the lipid molecular area A is determined, a parameter central to bilayer structure. For both X-ray and neutron scattering, A is calculated using the bilayer's thickness and additional volumetric information. However, it should be emphasized that the two scattering

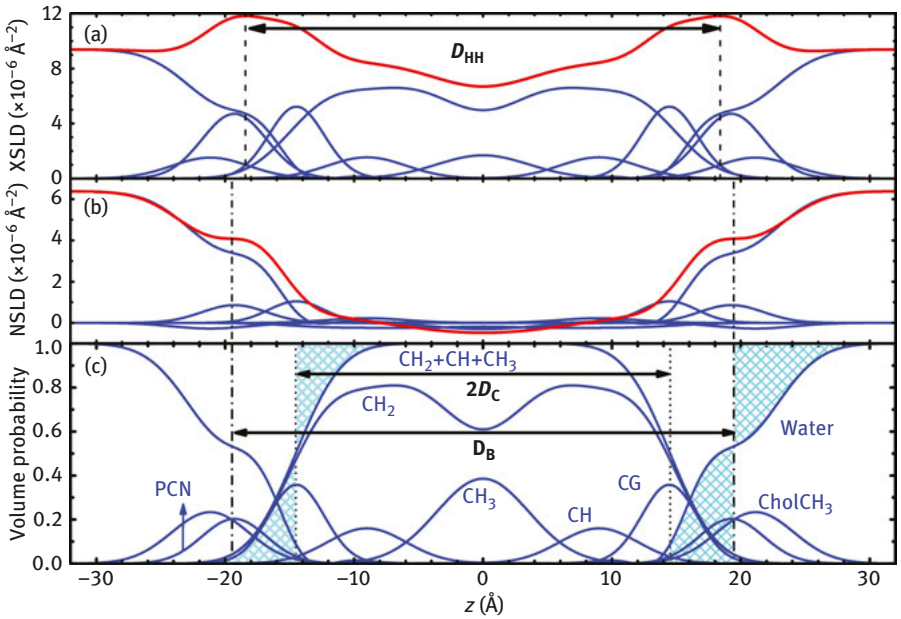

Figure 1.1: Illustration of lipid bilayer structure determination through the joint refinement of X-ray and neutron scattering data. The scattering density profile (SDP) representation of a bilayer in real space is shown, where the top panels show X-ray scattering length density (XSLD) with amplitudes calculated from the number of electrons and electron radius (**a**), and neutron scattering length density (NSLD) based on neutron coherent scattering amplitudes (**b**) of lipid component distributions. The total scattering length densities are denoted by the thick red lines. Panel (**c**) shows volume probability distributions, where the total probability is equal to 1 at each point across the bilayer. The locations where the shaded areas are equal define the Gibbs dividing surface between the bilayer headgroup and hydrocarbon regions (effectively D_C), and that between the lipid bilayer and the water phase (effectively $D_B/2$).

techniques are sensitive to different bilayer thicknesses. The thickness best resolved by X-rays is the distance between the electron density maxima found in the lipid headgroup region, D_{HH}, while in the case of neutron scattering, the contrast variation technique allows finding accurately the total bilayer thickness, D_B. Even though they are the two most robust experimentally determined parameters, D_{HH} and D_B are not directly comparable and neither measure on its own contains all of the desired bilayer structural information.

Area per lipid A follows from the volume probability underlying universally both of the scattering density profiles. The volume probability gives the Gibbs dividing surfaces for the water region and for the hydrocarbon region shown in Figure 1.1 and defined to be at $D_B/2$ and D_C, respectively. The parameter D_B, also known as the Luzzati thickness [20], impacts the model structure through the water distribution. It is defined by the equality of the integrated water probabilities $P_W(z)$ to the left of this surface and the integrated deficit of water probabilities to the right

$$\int_0^{D_B/2} P_W(z)\mathrm{d}z = \int_{D_B/2}^{d/2} (1 - P_W(z))\mathrm{d}z,$$

where $d/2$ is a point beyond which $P_W(z) = 1$, that is, a point beyond the furthest atom belonging to the lipid. From this, D_B can be expressed in the form

$$D_B = d - 2\int_0^{d/2} P_W(z)\mathrm{d}z.$$

Finally, the latter integral is equivalent to the integrated deficit of lipid probability and is equal to $d/2 - V_L/A$, where V_L is a total lipid volume. The equation then yields the first of the following equalities:

$$A = \frac{2V_L}{D_B} = \frac{(V_L - V_{HL})}{D_C}.$$

The second equality in the equation follows from the equivalent derivation applied to the dividing surface between the hydrocarbon and headgroup regions (V_{HL} being a volume of headgroup region). Even though the experimentally obtained scattering data contain information about the bilayer's structure in the z direction (along the bilayer normal), the above derivation allows us to evaluate the structure in the lateral direction, namely A. It should be emphasized that while the latter part of this equation was widely employed in X-ray scattering models, the first equality has important implications in the case of neutron scattering [21]. For protonated lipid bilayers dispersed in D_2O, neutrons are particularly sensitive to the overall bilayer thickness D_B. The previous equation thus directly yields lipid area from highly precise measurements of V_L. The simultaneous analysis of X-ray and neutron scattering data results in robust structural parameters that describe all the key bilayer features.

Biological activities of surface-active compounds are known to depend on lipid acyl chain length [22]. An exciting possibility is that the biological membrane has at its disposal a wide range of lipid lengths to stimulate membrane proteins at different locations. Intuitively, the length of a bilayer's acyl chains affects, to first order, bilayer thickness. Unfortunately, bilayer thickness values reported in literature, even in the case of given lipid bilayers, vary widely depending on the experimental method and analysis model [20] and prevent thus drawing any conclusions. However, the series of bilayer thickness parameters that are placed on a relative scale reveal conveniently such effect of acyl chain length [13]. Figure 1.2a shows a universal increase of bilayer thickness upon the extension of lipid acyl chain for lipids of various chemical compositions in the lipid headgroup region (i.e., PC vs. PG vs. PE lipids) and acyl chain region (i.e., fully saturated vs. monounsaturated vs. mixed chain lipids). In addition, the results showed no thermal effect to the chain length imposed thickness changes [13].

Figure 1.2a supports the notion that a change in the acyl chain length increases bilayer thickness similarly in the different bilayers. However, this is only part of the

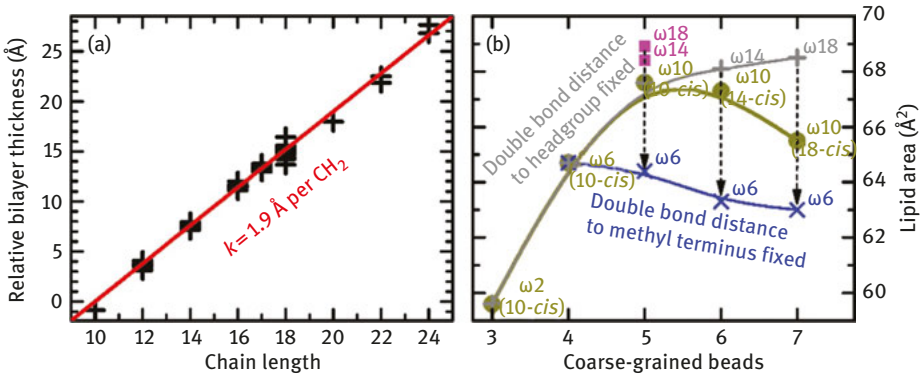

Figure 1.2: (**a**) Relative bilayer thicknesses as a function of chain length for lipids with different headgroups, acyl chain unsaturation, and temperature taken from the literature (see [13]). The slope of the linear function suggests a universal bilayer thickness increase of 1.9 Å for each CH_2 group (note the distance between the groups corresponds to half this number since the bilayer is spanned by two lipid molecules). (**b**) Area/Lipid obtained from coarse-grained MD simulations of systems corresponding roughly to the systems of diC12:1PC, diC16:1PC, diC20:1PC, diC24:1PC, and diC28:1PC (dark yellow solid dots) that are commonly utilized for modeling monounsaturated PC lipids. Gray plus signs, on the other hand, follow the results for systems with double bond position fixed at the third bead from the headgroup (i.e., 10-*cis*), and blue crosses those where the double bond was fixed with respect to the methyl terminus (i.e., *ω6* position). Dashed arrows indicate points where double bonds were shifted away from the lipid headgroup region, toward the bilayer center. All points are labeled with the double bond position, while due to the coarse-grained nature of the MARTINI model, the mapping between total number of carbons and double bond position is somewhat arbitrary [23]. Results are adapted from Kučerka et al. [13] and Kučerka et al. [24].

story. Another significant change takes place in the plane of the bilayer, namely the change to the area per lipid [25]. As a first approximation, one can estimate the behavior of *A* from the fact that bilayer thickness increases linearly with each additional carbon and so does lipid volume. However, this turned out to underestimate the values when compared to experimental results [26], demonstrating that it is not possible to simplify changes in the lateral direction in the same way that one does in the transverse direction. It therefore seems that lipid areas are strongly dependent on the acyl chain and headgroup compositions. Indeed, the fine balance between attractive and repulsive intrabilayer forces in the unsaturated lipid bilayers has been explained in terms of double bond position by the coarse-grained molecular dynamics simulations [24]. Figure 1.2b reveals an increase in area when the double bond's distance is fixed relative to the lipid's headgroup, whereas it decreases when the double bond is fixed relative to the bilayer center. As discussed previously [27], increased hydrocarbon chain length results in increased van der Waals attraction, which in turn leads to an ordering of the hydrocarbon chains that effectively reduces the area/lipid. However, lipid chain disorder also depends on double bond position, and it apparently has the largest effect when the double bond is located in the middle of the hydrocarbon chain [28].

The origin of different behavior between bilayer thickness and area per lipid as a function of acyl chain length is born by the forces that are responsible for minimizing the system's total energy. A simple formulation of the free energy for a planar bilayer involves attractive components that are the result of hydrophobic forces within the hydrocarbon chain region, headgroup dipolar interactions, and the repulsive components including steric interactions, hydration forces, and entropic effects due to acyl chain confinement [29]. In this, the interplay between the lateral interactions and headgroup chemical diversity documents why lipid areas likely play a central role. For example, the largest areas are observed for PG lipids even though PG does not possess the largest headgroup. This is however consistent with the observation that the introduction of anionic PG lipids results in decreased membrane stability [30]. The larger areas of PG lipids can also play important roles in regulating protein translocation [31], modulating bacterial membrane permeability [32], and enhancing membrane protein folding [33]. In contrast, structural studies of PE bilayers show a low number of water molecules hydrating their headgroups (between 4 and 7, compared to ~12 for a typical fluid PC bilayer). In fact, the steric exclusion interactions and strong hydrogen bonding between PE headgroups that are responsible for such low levels of hydration are unique among the glycerophospholipids. When compared to PC headgroups with strong repulsive interactions below areas of ~48 $Å^2$ preventing them achieving the minimal packing of their acyl chains (minimal area of an all-*trans* chain is ~20 $Å^2$) [34], the chains of DLPE, with its gel phase area ~41 $Å^2$ [35], appear to achieve such packing. The fluid phase PE area most likely represents the packing limit for fluid chains that is dictated completely by chain interactions, as opposed to the prevailing head–head interactions found in the other classes of lipids

[29]. The discussed structural results support the notion that lipid headgroups govern bilayer packing, while their properties are fine-tuned through the composition of their lipid acyl chains [13].

When scrutinizing the consequences of increased acyl chain length in the fully saturated bilayers, the evidence for an extended linear dependence of areas in Figure 1.3a was observed experimentally [26]. The decreased lipid area as a function of increasing chain length implies a smaller increase of the entropic contribution resulting from rotational isomerization (i.e., chain disorder), compared to the hydrophobic and van der Waals interactions in saturated chain lipids (diCn:0PC). On the other hand, increase in lipid area can be caused by the increased probability of *trans*-gauche isomerization that also happens to increase with chain length and temperature. Figure 1.3a shows the differences between the chain length dependencies for saturated and mixed chain lipids (diCn:0,18:1PC). As discussed above, the presence of a *cis*-double bond perturbs the packing of the hydrocarbon chains, which results in increased chain disorder and a concomitant increase in lipid lateral area. The addition of two methylene groups to mixed chain lipids then results in an increased area/lipid (blue symbols in Figure 1.3a), in contrast to the decrease experienced by saturated hydrocarbon chain lipids (black symbols in Figure 1.3a). This again suggests that rotational isomerization has a much more pronounced effect on lipid areas of unsaturated chain lipid bilayers than attractive van der Waals interactions. Importantly, the theoretically observed dependence on the position of double bond in Figure 1.2b is well reiterated for mono-unsaturated lipid bilayers (diCn:1PC) experimentally (dark yellow symbols) in Figure 1.3a.

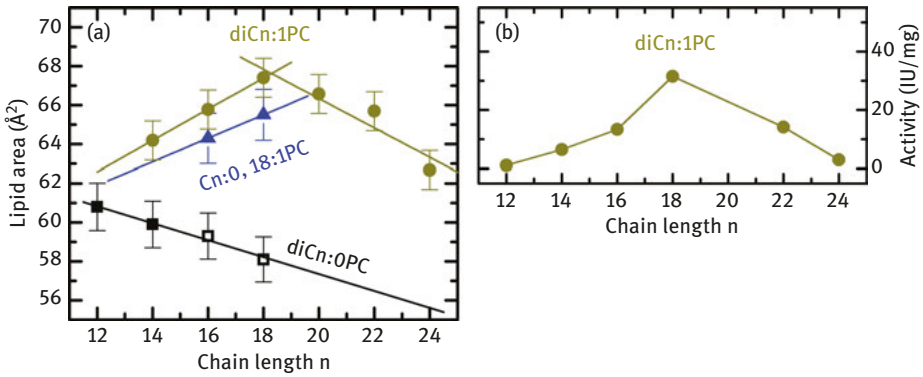

Figure 1.3: (**a**) Area per lipid as a function of hydrocarbon chain length for the various PC lipids at 30 °C. Saturated fatty acid chains are denoted by black squares, while blue triangles and dark yellow circles denote the presence of one or two mono-unsaturated fatty acid chains, respectively. All areas shown by solid symbols are obtained using 30 °C data, while areas indicated by open squares are calculated from fluid phase data using the appropriate thermal area expansivities (from Kučerka et al. [26]). (**b**) The dependence of specific Ca^{2+}-ATPase activity at 37 °C as a function of hydrocarbon chain length of mono-unsaturated PC lipids to which it was reconstituted from Karlovská et al.[27].

The above-discussed results also suggest importantly that lipid area is a good indicator of the lateral interactions within the bilayer. This is further corroborated by an activity of Ca^{2+}-ATPase reconstituted into lipid bilayers that was found to depend on various structural parameters such as thermodynamic phase, structure and charges of polar headgroups, and of the utter importance the hydrocarbon chain length [27]. The results displayed in Figure 1.3b indicate almost exactly the same dependence of ATPase activity on the lipid chain length as was observed in the case of lateral area in bilayers made of the same mono-unsaturated lipids (Figure 1.3a). Enzymatic activity was found to be maximal in bilayers composed of diC18:1PC lipids, and decreased, as much as fourfold, in both shorter and longer chain lipid bilayers. The structural data obtained via scattering techniques thus point to a decrease of membrane lateral pressure as a very likely mechanism of stimulating and/or quenching membrane incorporated proteins that provide it with an active function.

Bilayer membranes are characterized by large lateral stresses born by the above-mentioned interactions and depending on the depth within the membrane [36]. The balance of repulsive and attractive forces in the interfacial region is dictated for the most part by the chemical composition of lipid headgroups, as discussed above. The repulsive interactions within the hydrophobic region are then closely related to the chain length and its unsaturation, thus the dynamics of hydrocarbon chains [37]. Interestingly, such interactions may affect not only the proper function of large integral membrane proteins, but the integration and location of other small components of the membrane. For instance, molecular dynamics simulations have shown that the angle of cholesterol with respect to the bilayer normal varies with the number of double bonds present in the lipid fatty acid chains [38] and/or the bilayer thickness [39]. The results showed that the frequency of cholesterol's flip-flop between bilayer leaflets dramatically increases with the increasing disorder of lipid chains. Recently, neutron studies of deuterated cholesterol incorporated into polyunsaturated fatty acid (PUFA) bilayers found cholesterol sequestered inside the membrane, in contrast to its usual position with the hydroxyl group located near the lipid/water interface [40–42].

The average position of cholesterol molecules within the bilayer could be handily deduced from neutron diffraction experiments when labeling the parts of cholesterol with deuterium atoms. The hydrogen/deuterium substitution, for the most part, does not change the chemical and structural properties of the biologically relevant systems, while the differential sensitivity of neutrons to hydrogen and deuterium allows to increase the sensitivity of neutron scattering experiments considerably. The Fourier reconstruction results straight-forwardly in the NSLD calculated from experimental scattering form factors F_h as

$$\mathrm{NSLD}(z) = \left(\frac{1}{d}F_0 + \mathrm{NSLD_W}\right) + \frac{2}{d}\sum_{h=1} F_h \cos\left(\frac{2\pi hz}{d}\right),$$

which consists of nonlabeled parts of hydrated membrane (M) and the parts labeled (L) with deuterium (D) in the case of labeled sample

$$\mathrm{NSLD_D}(z) = \mathrm{NSLD_M}P_\mathrm{M}(z) + \mathrm{NSLD_D}P_\mathrm{L}(z),$$

or "labeled" with hydrogen (H) in the case of nonlabeled sample

$$\mathrm{NSLD_H}(z) = \mathrm{NSLD_M}P_\mathrm{M}(z) + \mathrm{NSLD_H}P_\mathrm{L}(z).$$

The subtraction of the two NSLD profiles then includes only the probability distribution of labeled components

$$P_\mathrm{L}(z) = \frac{\mathrm{NSLD_D}(z) - \mathrm{NSLD_H}(z)}{\mathrm{NSLD_D} - \mathrm{NSLD_H}}.$$

The resulting difference NSLD profile obtained solely from experiment can provide the distribution of the label with nanometer resolution that is directly comparable to molecular modeling utilizing simulations [16]. Figure 1.4a and b portray such approach in the case of cholesterol-loaded PUFA bilayers.

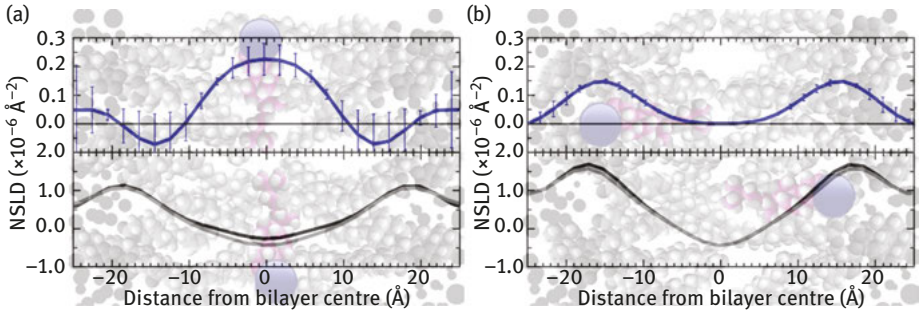

Figure 1.4: Neutron scattering length density (NSLD) profiles in bottom panels and their differences (deuterated minus nondeuterated cholesterol) in top panels show the distribution of cholesterol's deuterium label (depicted by a big blue sphere in the background schematics). It is found in the center of highly disordered bilayers (**a**), while cholesterol orients in its canonical orientation in the case of more ordered bilayers (**b**).

The samples in the neutron diffraction experiments are typically prepared on the flat substrate for an unambiguous differentiation between the direction perpendicular and parallel to the membrane plane [43]. This allows, in addition, the very same sample to be reproducibly measured in different contrast conditions when hydrated through water vapor phase. Samples hydrated with 100% D_2O are best suited for the determination of the bilayer's overall structure (i.e., total thickness, area per lipid, etc.) because of the excellent contrast provided between the hydrating medium and the bilayer [19]. On the other hand, fine structural details are more obvious in samples

hydrated with 8 mol% D_2O, where the water contribution has a net zero NSLD and the bilayer structure is not obscured by scattering from the solvent. Nevertheless, all the difference profiles obtained from samples hydrated with various percent D_2O solutions should result in the same distribution function. This is due to the fact that both the NSLD associated with the lipid and that of the hydrating medium are subtracted with the end result corresponding to the difference between the labeled and unlabeled sample NSLDs (i.e., six deuterium minus six hydrogen atoms per cholesterol molecule) [44].

The results shown in Figure 1.4 clearly show cholesterol's two very different orientations in different bilayers [45]. The central location for cholesterol is observed in Figure 1.4a for PUFA bilayers doped with up to 30 mol% palmitoyl-oleoyl-phosphatidylcholine (POPC). The increasing amount of more ordered lipid however allows to change the cholesterol's orientation when PUFA bilayers contain more than 50 mol% POPC. The deuterium label in Figure 1.4b appears to be approximately 15 Å from the bilayer center, placing cholesterol's hydroxyl group within the bilayer's hydrophobic/hydrophilic interfacial region. This observation confirms the notion that cholesterol's orientation can be altered by modifying the profile of membrane lateral pressure through changing the ratio of PUFA/saturated chain lipids. Considering the lipid heterogeneity of biological membranes, this result may be viewed as a prerequisite for the mechanism by which cholesterol transports through the cell membrane. It is even possible to imagine the aversion that certain lipids have for each other to drive the formation of functionalized domains with selective profiles of membrane lateral pressure.

1.3 The effect of cholesterol on model membranes

In a further support of the role of membrane lateral pressure, it is interesting to note that activity of Na,K-ATPase discussed previously was shown to be sensitive not only to phospholipid chain length but also to cholesterol content [46]. Maximal protein activation was seen in long-chain phospholipids in the absence of cholesterol, while it shifted toward medium-chain phospholipids in the presence of cholesterol. This observation clearly suggests that not only the lipid species affect the orientation of cholesterol in membranes but that cholesterol alters the structure of bilayers. However, it is not clearly resolved whether the cholesterol affects the lateral packing of lipids [47], or it alters the hydrophobic matching between the lipid and protein [27]. In binary lipid/cholesterol mixtures, cholesterol's addition to fluid phase lipid bilayers results in increased acyl chain order [9–13], while having the opposite effect on lipid headgroups. The consensus of many studies, including NMR [14, 15], EPR [16, 17], and fluorescence [18], is that cholesterol acts as a "spacer" molecule, increasing the separation between lipid headgroups, thereby reducing possible

interactions between them. These studies further demonstrate that while the addition of cholesterol decreases the extent of water penetration into the membrane's hydrophobic region, there is a concomitant increase in headgroup hydration.

When it comes to SANS experiments, data analysis has traditionally been based on the Kratky–Porod approximation, or by fitting the data to a simple single-strip model of the bilayer [21, 22, 36–38]. Although this approach is rather popular, it neglects the inner structural details of the bilayer. More accurate models to analyze SANS data [29, 39] were inspired by the results from molecular-dynamics simulations, which show additional substructure within the bilayer. The full form of scattered intensity measured for the dilute system of polydisperse unilamellar vesicles (ULVs) can be calculated as the square of the planar bilayer form factor $F(q)$ (q is the scattering vector $q = 4\pi \sin(\theta/\lambda)$, while 2θ is the scattering angle and λ is the neutron wavelength) and multiplied by the function which includes the particle's sphericity and the system's polydispersity as follows [48]:

$$I(q) = F^2(q)\frac{8\pi^2(z+1)(z+2)}{s^2q^2}\left\{1-\left(1+\frac{4q^2}{s^2}\right)^{-(z+3)/2}\cos\left[(z+3)\arctan\left(\frac{2q}{s}\right)\right]\right\},$$

where $s = R_m/\sigma_R^2$ and $z = R_m^2/\left(\sigma_R^2 - 1\right)$ are the products of the ULV's mean radius R_m and its polydispersity σ_R (i.e., the width of the size distribution function). The bilayer form factor $F(q)$ is the well-known Fourier transform that for centro-symmetric profile is written as

$$F(q) = 2\int_0^{d/2}[\mathrm{NSLD}(z) - \mathrm{NSLD}_W]\cos(qz)\mathrm{d}z,$$

where $NSLD_W$ is the neutron-scattering length density of water solvent that acts as a background in the sample. The bilayer's profile NSLD(z) can be further separated according to various multishell schemes [49]. Of particular importance in this development was the replacement of a sharp water–bilayer interface by a "smooth" one [50]. This function consists of a linear term for the distribution of water penetrating the headgroup (see Figure 1.5a).

There are two sets of parameters that determine the entire SANS curve: in the low-q region, scattering is sensitive to large length scales, that is, the overall size of the ULVs, while the information about bilayer structure is contained in the mid- and high-q regions (see Figure 1.5b). Two parameters describe the size distribution function of ULVs (i.e., mean radius and the width of its distribution), while two others define the bilayer model (i.e., area per lipid and amount of penetrating water). In addition, there are two linear parameters corresponding to a multiplicative scaling coefficient and an additive background constant. In total, there are six fitting parameters, which reach the limitation of standalone SANS data analysis [49] (in contrast to SANS and SAXS-combined approach discussed above). Structural parameters are refined in terms of an iterative model-fitting approach, which result in the bilayer profile.

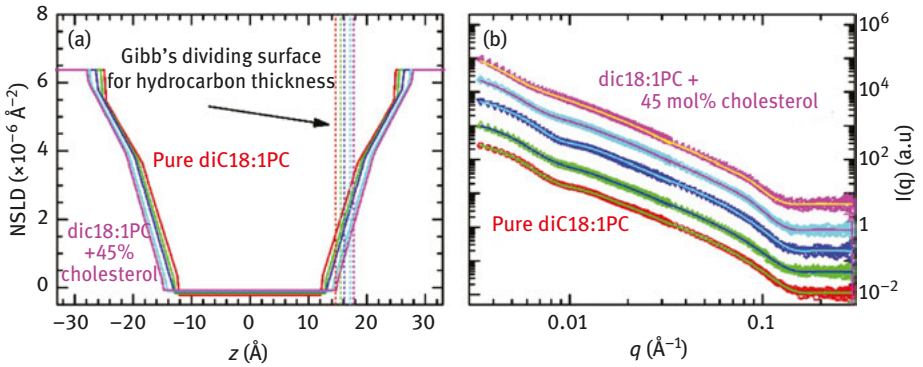

Figure 1.5: (**a**) Neutron scattering length density (NSLD) profiles of lipid bilayers made of diC18:1PC and various amounts of cholesterol (0, 17, 29, 38, and 45 mol%). The model comprises constant NSLD for hydrocarbon chains in the bilayer center, while linear functions describe the gradual increase of water molecules penetrating the lipid headgroup region. The dashed lines depict the Gibb's dividing surface between headgroup and hydrocarbon regions. (**b**) Small-angle neutron scattering (SANS) curves showing the experimentally measured intensities (points) for bilayers in the form of unilamellar vesicles (ULVs). Solid curves represent the fitting results of models shown in panel A. Adapted from Kučerka et al. [50].

Figure 1.5a shows the characteristically large contrast observed between the hydrocarbon region in the bilayer center and solvent outside. The contrast gradually decreases within an interfacial region until the boundary between the lipid headgroups and water is reached. All NSLD profiles show this behavior, typical of protonated phospholipid bilayers dispersed in D_2O. In addition, the bilayer properties are continuously changing also as a function of cholesterol content. First, there are increases to the hydrocarbon NSLD with increasing amounts of cholesterol – although this change is very small because of the cholesterol and the lipid hydrocarbon region having similar NSLDs. Second, the monotonically increasing bilayer parameters in Figure 1.6a and b with cholesterol content serve a direct observation of cholesterol-induced increases to the hydration of the lipid headgroup region. Most importantly, however, results in Figure 1.6c and d show definite increases in bilayer thickness as a function of cholesterol concentration [50]. The rigid hydrophobic molecule of cholesterol in an obvious way increases the thickness of the hydrocarbon chain region in the case of shorter lipid bilayers. However, cholesterol may be expected to increase or decrease the thickness of the hydrocarbon chain region in the case of long-chain lipid bilayers. The observations of a thickening of the hydrocarbon chain region, even for diC22:1PC bilayers, imply then that cholesterol prefers to further order the lipid's hydrocarbon chain over the possibility of rectifying the hydrocarbon chain mismatch [39, 50]. Cholesterol promotes the formation of a liquid-ordered phase by condensing the bilayer along its lateral direction.

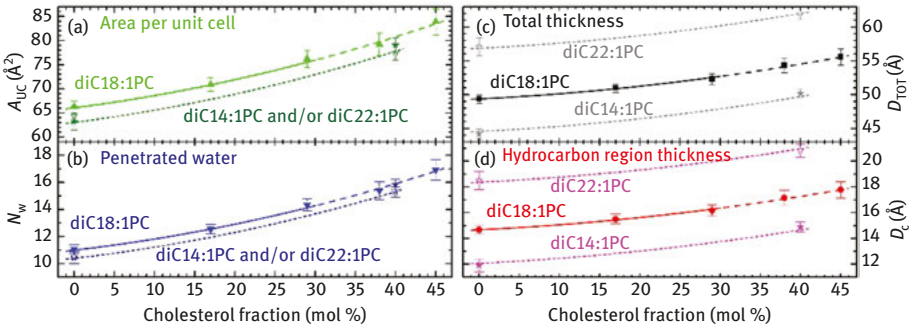

Figure 1.6: Bilayer parameters plotted as a function of cholesterol concentration for three mono-unsaturated phospholipids with different chain length. All the parameters [i.e., area per lipid (**a**), and amount of water molecules penetrating the lipid headgroup region (**b**), total bilayer thickness (**c**), and that corresponding to the hydrocarbon region (**d**)] exhibit monotonic dependencies as functions of cholesterol concentration. The uniform behavior in the case of different chain length lipids suggests the same mechanism for the cholesterol's effect on these membranes. Adapted from Kučerka et al. [50].

SAXS experiments, although missing the high contrast available in the case of previously discussed SANS, can benefit from highly brilliant modern synchrotron sources. Consequently, SAXS data often provide higher resolution when compared to that of SANS measurements, and they may reveal additional structural results. For example, SAXS experiments can detect an asymmetric distribution of lipid densities across the bilayer. In this case, bilayer asymmetry is readily detectable because of the distinct scattering features associated with the effect. The scattering from symmetric structures is characterized by periodic oscillations that cross zero and result thus in typical zero minima in the scattered form factors [51, 52]. A lack of zero intensity, on the other hand, indicates bilayer asymmetry, as can be deduced from the complete form of the Fourier transform with a complex exponential

$$I(q) \approx \left[\int_{-d/2}^{d/2} [\mathrm{XSLD}(z) - \mathrm{XSLD_W}] \cos(qz) \mathrm{d}z\right]^2 + \left[\int_{-d/2}^{d/2} [\mathrm{XSLD}(z) - \mathrm{XSLD_W}] \sin(qz) \mathrm{d}z\right]^2.$$

It was shown, based on this experimental approach, that the addition of 44 mol% cholesterol results in some of the bilayers (i.e., $n = 14$, 16, and 18) to become asymmetric, where cholesterol was found to distribute unequally between the bilayer's two leaflets [53]. The subtle changes in the total XSLD shown in Figure 1.7 reveal the asymmetry-related sharpening of the lipid-component distributions in the cholesterol-depleted side, while their broadening in the cholesterol-enriched side [39]. The MD simulations corroborated the effect of bilayer asymmetry on the scattering form factors (namely, the "lift-off" in the first minimum) and provided further details. By

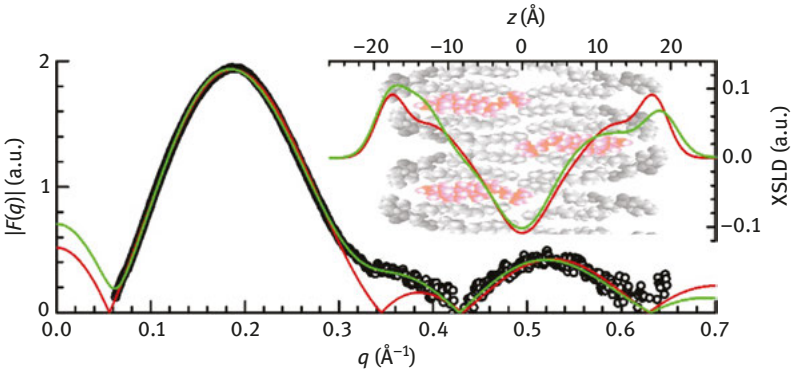

Figure 1.7: X-ray scattering form factors $F(q)$ obtained for diC14:1PC bilayers with 44 mol% cholesterol. The insert shows 1D XSLD profiles in the forefront of bilayer schematics depicting an unequal distribution of cholesterol (magenta) between the two bilayer leaflets. The red curves are best fits to the data using a symmetric bilayer model, while the green curves are best fits to the data using an asymmetric model.

varying the degree of cholesterol asymmetry in each case, the degree of asymmetry was established by matching the magnitude of the experimentally observed "lift-off." The best match with the ULV experimental data provided a final cholesterol distribution corresponding to the ratio of 51/29 [39]. It seems that cholesterol, by distributing itself unequally between the bilayer's two leaflets, induces bilayer asymmetry in symmetric bilayers whose hydrocarbon chains contain up to 18 carbons. It is interesting to note that the magnitude of bilayer asymmetry coincides with the difference in length between the lipid's hydrocarbon chains and cholesterol. Asymmetry is most pronounced in the thinnest bilayer (i.e., diC14:1PC) whose hydrocarbon thickness is significantly shorter than a cholesterol molecule. With decreasing hydrophobic mismatch, however, there is a decrease in cholesterol's asymmetric distribution, eventually distributing itself equally between the two leaflets of diC20:1PC bilayers. This suggests that symmetric bilayers are formed when the bilayer's hydrocarbon thickness is close to the length of cholesterol. It is possible that, in addition to bilayer disorder discussed above, hydrophobic mismatch is after all another important factor when lipids are mixed with other membrane components.

The membrane's composition and the inclusion of small molecules, such as cholesterol discussed above, alter the membrane's structure and physical properties, which in turn affect its various functions. Recent studies have shown the lipid membrane to be extremely important also in enabling amyloid fibril formation and its ensuing toxicity [54, 55]. The formation of insoluble amyloid fibrils composed of proteins in β-sheet conformation found on the surface of neuron plasma membrane is a fingerprint of Alzheimer's disease (AD) and various others related to protein conformational disorders. In this, cholesterol has been shown to enhance the amyloid

binding and fibril formation when present in a membrane [56, 57]. In opposite to cholesterol that is mostly hydrophobic, membrane can accommodate also hydrophilic molecules. One example is melatonin – a pineal hormone that is produced in the human brain during sleep and that sets the sleep–wake cycle (and circadian rhythm) [58]. Intriguingly, it has been suggested to have a protective role against amyloid toxicity [59, 60], while the underlying molecular mechanism of this protection is not well understood. It may involve a nonspecific interaction of the molecule with the membrane and decreasing the gel-to-fluid phase transition temperature by increasing the membrane disorder [61–64]. It has been also shown that melatonin may compete with cholesterol for binding to lecithin and that it may even displace cholesterol from the phospholipid bilayer [65]. Melatonin's ability to control cholesterol content, ergo membrane rigidity, may thus reduce the effects of cholesterol on the membrane, as well as cholesterol-mediated processes [66].

In order to better understand how melatonin and cholesterol affect the interaction of biomolecules with the membrane, it is necessary to systematically determine the effects that these molecules have on membrane structure. Small-angle neutron diffraction (SAND) experiments allow for the *in situ* manipulation of sample conditions but, more importantly, provide quantitative data on the distribution of structural moieties, their sizes, shapes, and correlation lengths [67]. Variations in diffraction maxima (see Figure 1.8a) can signal important changes to membrane structure, which,

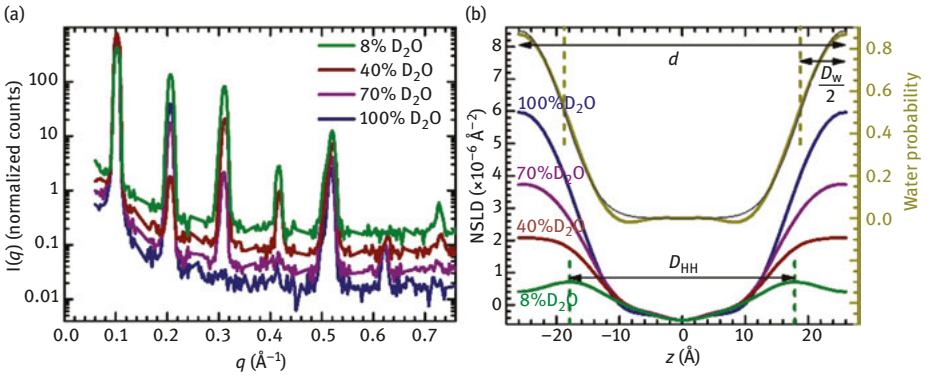

Figure 1.8: (**a**) Small-angle neutron diffraction curves recorded for lipid bilayers hydrated with different D_2O/H_2O water vapor. Note the vertical shift between the various curves introduced for the clarity of presentation. (**b**) Neutron scattering length density (NSLD) profiles of lipid bilayers calculated in various D_2O/H_2O contrast conditions scaled according to the left-hand axis. The distance between two peaks corresponding to lipid headgroups is obtained from 8% D_2O profile (green color), and it defines the thickness parameter D_{HH}. The dark yellow curve (scaled according to the right-hand axis) shows the profile of water probability distribution across the bilayer, describing thus the water encroachment (central position is depicted by broken lines). The gray line represents the error function fit to the distribution calculated from experimental data. The total interlamellar spacing is shown by d and the thickness of water layer between adjacent lipid bilayers is depicted by D_W.

in turn, may have biological implications. With regard to structural biology, the various scattering techniques complement crystallographic studies that, in many cases, require hard-to-obtain, high-quality crystals of macromolecules. Due to the intrinsic disorder present in biomimetic systems – disorder that is considered important for the proper function of biological systems – the vast majority of membrane samples do not form perfect, or even near perfect crystals, that are needed to solve structure to atomic resolution. The limited amount of attainable data from such samples is then best described by broad statistical distributions and membrane overall characteristics. For example, in the case of model membrane systems (i.e., positionally correlated structures), the position and amplitude of Bragg reflections reveal the membrane's lamellar periodicity (d) and one-dimensional NSLD profile (Figure 1.8b). Further, by changing the system's "contrast" through the exchange of H_2O for D_2O, it is possible to determine the extent that water penetrates into the bilayer [68]. In fact, such contrast variation approach is the only direct method that allows to solve the infamous scattering phase problem without disturbing the sample structure [69, 70]. Consequently, the distribution profile of water penetration is inferred from difference NSLD profiles obtained at various contrast conditions. It first parses each NSLD(z) into contributions corresponding to the membrane (M) and water (W) molecules

$$\mathrm{NSLD}(z) = \mathrm{NSLD}_\mathrm{M} P_\mathrm{M}(z) + \mathrm{NSLD}_\mathrm{W} P_\mathrm{W}(z),$$

while it considers the two probabilities being contrast independent and satisfying the spatial conservation principle (i.e., $P_\mathrm{M}(z) + P_\mathrm{W}(z) = 1$ at each point z across the membrane). Since NSLD_M does not depend on external contrast conditions, the subtraction of NSLD profiles measured at two different D_2O contents includes only the probability of water, which can be expressed as

$$P_\mathrm{W}(z) = \frac{\mathrm{NSLD}_1(z) - \mathrm{NSLD}_2(z)}{\mathrm{NSLD}_\mathrm{W1} - \mathrm{NSLD}_\mathrm{W2}}.$$

The water probability $P_\mathrm{W}(z)$ is between 0 and 1 if $\mathrm{NSLD}_1(z)$ and $\mathrm{NSLD}_2(z)$ are obtained on an absolute scale [68], and it provides an encroachment of water in a comparison to the membrane profile (see Figure 1.8b). As discussed previously, NSLD distribution corresponds to the membrane profile directly if obtained at 8% D_2O. The resulting profile is then characteristic of two peaks representing the opposing lipid headgroups of the bilayer, and their distance (D_HH) provides one of the membrane thickness parameters (see Figure 1.8b).

Membrane thickness is a structural parameter that is directly related to lipid–lipid and lipid–protein interactions in biomembranes. The experimental results in Figure 1.9 confirm the previously reported and well-known bilayer thickening effect induced by cholesterol. This manifestation of cholesterol in bilayer thickness can be interpreted as a disorder–order transition of the lipid's acyl chains. The hydrocarbon chains experience increased order due to their interactions with the rigid cholesterol molecules. Interestingly, the experimental results show also that the addition of melatonin has the

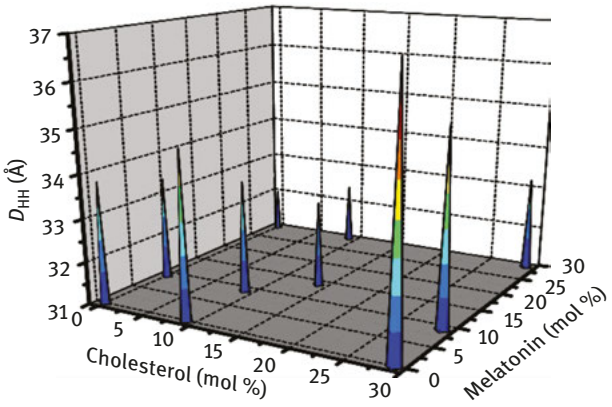

Figure 1.9: Head-to-head distance D_{HH} obtained from NSLDs of diC18:1PC bilayers loaded with various amounts of cholesterol and melatonin. Bilayer thickness clearly increases with an increasing amount of cholesterol, while it decreases upon the addition of melatonin which counteracts the effect of cholesterol.

exact opposite effect, that is, melatonin causes bilayer thinning [71]. This result suggests that melatonin incorporates itself into the bilayer's headgroup region and acts as a spacer therein. According to this scheme, melatonin increases the free volume in the bilayer's hydrocarbon region. This free volume is then readily taken up by the disordered chains at the expense of their effective length (i.e., reduction of bilayer thickness). This notion is also supported by the encroachment of water molecules deeper into the membrane, as readily extracted from contrast varied SAND measurements [71].

The effect of melatonin and cholesterol on model lipid bilayers was corroborated by MD simulations [71]. In agreement with the experimental SAND data, MD simulations show that cholesterol increases the acyl chain order in lipid bilayers, while melatonin decreases this order. In other words, melatonin increases the fluidity of the membrane due to its preferred location just inside the crossover region describing the lipid headgroups and the fatty acid chains. Both experimental and theoretical data are in good agreement and show that the effect of melatonin on bilayer thickness is opposite to that of cholesterol. These observations may prove to be important for other studies on amyloid toxicity, as they may lend some insight into understanding the molecular mechanism of melatonin's protection in AD. For example, melatonin levels in the body have been shown to decrease with age [72]. As AD is more prevalent later in life, the effects of melatonin and cholesterol on lipid membrane become increasingly important as their amounts in membranes also change with age. The conclusions of various investigations can, therefore, provide an understanding for the possible structural changes taking place within biological membranes.

1.4 Alcohol interactions with lipid bilayers

The proper functioning of biological membranes appears to be well correlated to the structural properties, thermodynamic conditions, and composition of lipid matrices. The various additives are known to enable or inhibit these functions provided, for the most part, by membrane proteins. The capacity of a substance to interact with biological membrane and modulate its functionality is defined by biological activity. In the case of molecules with long hydrocarbon chains, such biological activity is known to depend on the chain length. Intriguingly, it increases with increasing chain length up to a maximum, while it decreases again with further chain length increases. Such cutoff behavior has been observed in many cases of various drugs or toxins, suggesting the mechanism for this effect depending on the hydrophobic mismatch between the substance and lipid bilayer in the transmembrane direction, and/or corresponding interactions in the lateral direction [22]. General anesthetics are one of the typical examples displaying the cutoff effect.

Alcohols and other general anesthetics have been known to surgeons for over the century [73]. Despite their successful applications, however, the understanding of anesthesia mechanism is still lacking. According to the general consensus, the place of their action is being recognized either within proteins or lipid membrane [74–76]. However, the hypothesis based on the unspecific interactions between anesthetics and membrane lipids may be more plausible due to, for example, a wide spectrum of membrane proteins that are affected. In any of the two cases, the general anesthetics, including aliphatic alcohols, offer an exciting example on the structure–function correlation that is sought out in biological membranes. Amphiphilic molecules, like long-chain alcohols, intercalate into membranes and change their structural and/or dynamical properties, which in turn might affect membrane-bound protein conformations and result in protein functional changes that are involved in general anesthesia. Although it is not known which structural perturbations are responsible for these effects, it is evident that the exploration of the long-chain alcohol interactions with model membrane can contribute to a better understanding of the cutoff dependencies in various biological activities of homologous series of amphiphilic compounds [77, 78].

Neutron scattering techniques have proven to be valuable tools in structural biology, biophysics, and materials science due to their ability to provide a complex set of parameters. The most straightforward parameter obtained from diffraction measurements (such as shown in Figure 1.8a) corresponds to the lamellar spacing between repeating unit cells, d. It is inversely related to the position of Bragg diffraction peaks (q_h) as $d = 2\pi h/q_h$. Experimental results for oriented lipid multilayers in excess water then suggest the increase of total lamellar spacing upon the addition of the alcohols with their tail length increasing from 10 to 18 carbons [79]. The extension of changes is proportional to the alcohol's tail length, although the changes are relatively small (Figure 1.10a).

The total lamellar *d*-spacing in the case of hydrated membrane system consists of two components: the total thickness of lipid bilayer D_B and the thickness of water layer in-between the bilayers (see also Figure 1.8b). The water layer comes in as a result of interbilayer interactions that are characteristic to the given lipid composition and thermodynamic state including the hydration conditions. One of its particularly interesting contributions is determined by the membrane viscoelastic properties and it relates to the softness of membrane [80]. Literature results nevertheless show a marginal dependence of water layer thickness on the alcohol tail lengths, suggesting no changes to these characteristics [79]. Figure 1.10a then shows that major changes in these bilayer systems happen to D_B, and accordingly, it displays very similar trend to that of total lamellar *d*-spacing when examined as a function of tail length of the added alcohol. Interestingly however, there is also a significant difference in the behavior of the two thickness parameters. While the addition of any and all investigated alcohols increases the *d*-spacing, D_B is always smaller when comparing alcohol-loaded bilayers to neat DOPC bilayers. This can be seen in Figure 1.10a by a broken line being below the points in the case of *d*-spacing data, and it is above the points in the case of bilayer thickness. Obviously, the water layer increases upon the addition of any alcohols to the neat DOPC bilayers; yet, it stays mostly constant for alcohols with different tail lengths.

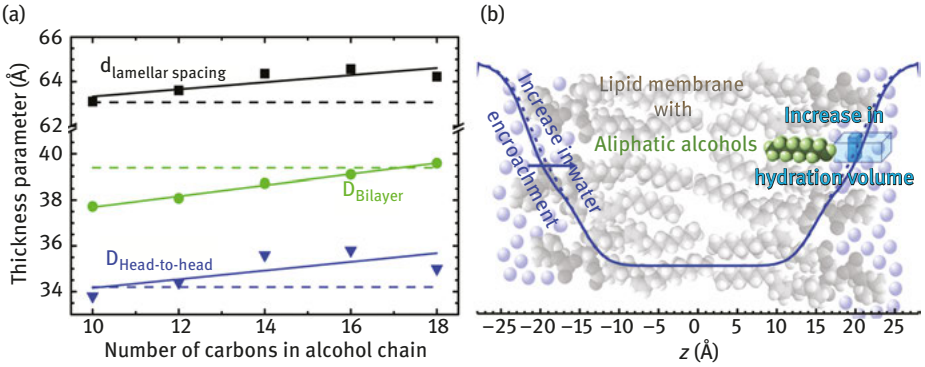

Figure 1.10: (**a**) Various bilayer thickness parameters obtained for neat dioleoyl-phoshatidylcholine (DOPC) bilayers (dashed lines) and those with the addition of 0.3:1 molar ratio of tail length varied alcohols (solid points). The total *d*-spacing of lipid multilayers in excess water (black color), the total bilayer thickness without interbilayer water layer (green color), and head-to-head distance obtained from NSLD profiles measured at 8% D_2O contrast conditions. The solid lines are linear approximations of data shown to emphasize the average changes. (**b**) Illustration of water encroachment shown by blue lines. Fewer water molecules penetrate the bilayer composed of neat DOPC (solid line) compared to the scenario with alcohol (depicted by green color) intercalating the bilayer (broken line). Water molecules (blue spheres) fill an additional space (the dark portion of a blue rectangle) resulting from increased water penetration and enlarged lateral area above the alcohol molecule. Adapted from Kondela et al. [79].

The above-discussed observations suggest the changes may be happening to the lipid headgroups. It is therefore beneficial to look closely at one more parameter extractable easily from SAND experiments. The fine structural details of systems dispersed in water are more obvious in samples hydrated with 8 mol% D_2O, as discussed already. Such obtained NSLD profiles provide directly the features related to lipid bilayer, where carbonyl–glycerol groups are typical of a pronounced maximum. The distance between the opposite maxima, thus in addition to providing yet another thickness parameter D_{HH}, allows to scrutinize the bilayer internal structure. D_{HH} plotted in Figure 1.10a shows a behavior that is very similar to that of total d-spacing. Considering that it is derived from the structure of bilayers themselves, while D_B relates to the water–bilayer interface, the combination of their changes points to differences in the encroachment of water molecules upon the addition of alcohols. The distances of both lipid headgroups and water–bilayer interface from the bilayer center increase accordingly to the tail length of intercalating alcohols. However, changes in D_B, relative to neat DOPC bilayers, are shifted toward the center by about 1 Å at each side of bilayer, when compared to the relative changes of D_{HH}. In other words, the addition of alcohols results in some of the space in the polar headgroup region (note also the expansion of lateral area upon the addition of alcohols [79]) being filled with extra water molecules (Figure 1.10b). This in turn contributes to the decrease of membrane lateral pressure in the region directly above alcohols and supports the modulation of membrane mechanical properties by general anesthetics as a likely mechanism of the anesthesia effect.

1.5 Cation-containing lipid membranes

Amongst the intramembrane interactions lipid–lipid, lipid–protein, and even protein–protein, the significance of the aqueous phase for the proper functioning of biological membranes cannot be overestimated. Plasma membrane properties such as membrane fluidity, bending and compressibility moduli, electrostatics, and aggregation and fusion are in addition associated with ions that are ubiquitous in the cytosol and the extracellular fluid. Not surprisingly, ions such as Na^+, K^+, Ca^{2+}, Mg^{2+}, Zn^{2+}, or Cl^- have been found to play a prominent role regarding bilayer structure. Their functions within cell membranes are understood to influence the gating of ion channels, membrane fusion, and membrane "fluidity" to name but a few [67]. Although a complete understanding of the physicochemical processes taking place in biomembranes has yet to be established, their functionality is known to depend strongly on the type of ion, the chemical composition of the membrane's interface, its thermodynamic state, and degree of hydration [81].

The different effect of monovalent versus divalent cations was observed in bacterial model membranes composed of lipopolysaccharides (LPS) utilizing SAND measurements [82]. Due to a particular sensitivity to the hydration conditions, the diffraction

data showed that water penetrates Ca^{2+}-loaded LPS bilayers to a lesser extent than those loaded with Na^{+}. While Ca^{2+} cations make LPS bilayers more compact and less permeable to water, a significant amount of water was found to penetrate deep into Na^{+}-LPS bilayers, including the bilayer's hydrophobic core center. In fact, the disappearance of diffraction peaks when liquid-crystalline Na^{+}-LPS multilayers were subjected to high levels of hydration (see Figure 1.11a) suggested that the deep water penetration increases up to a critical point, beyond which the long-range correlation of bilayer assembly is destroyed [83]. Such a destabilization mechanism could provide a general explanation of how nonlamellar phases are formed and how small molecules penetrate the outer membrane of gram-negative bacteria.

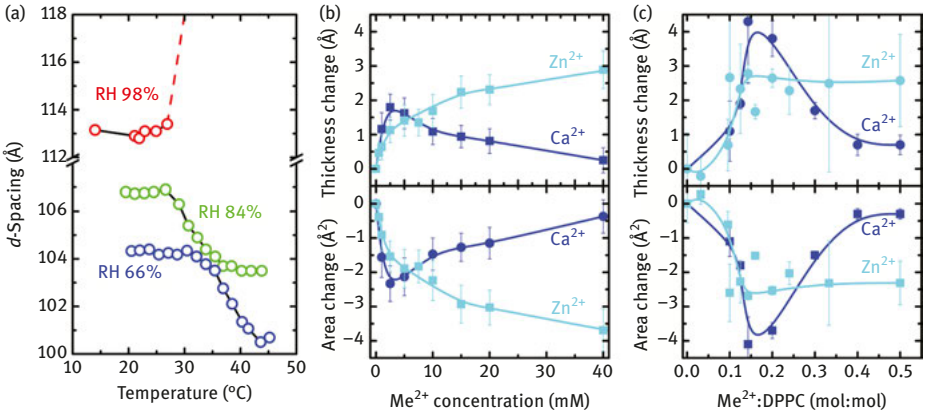

Figure 1.11: (**a**) Temperature dependence of the lamellar *d*-spacing at the various levels of relative humidity (RH) controlled externally. The multilamellar structure of Na^{+}-loaded LPS bilayers transitions from gel to liquid-crystalline phase at 66% and 84% RH. However, the repeating nature of the structure disappears when temperature increases above 28 °C at 98% RH. Zn^{2+} and Ca^{2+} cation-induced changes to bilayer structure expressed through the bilayer thickness, and area per unit cell A_{UC} obtained from SANS (**b**) and SAND (**c**) experiments. The A_{UC} comprises a DPPC molecule and the appropriate number of cations and is calculated from the inverse relation to the bilayer thickness (i.e., $A_{UC} = V_{UC}/D_{Bilayer}$). Changes are calculated with respect to neat DPPC bilayers. Results are adapted from Abraham et al. [83], Uhríková et al. [84], and Kučerka et al. [85].

The increased levels of hydration are most likely associated with an enhanced biological activity in the bacterial membranes and represent thus an intriguing research issue. The complexity of the system however does not allow for straightforward correlations of structural results. The effect of ions on the other hand can be revealed effectively utilizing model systems. For example, systems of dipalmitoylphosphatidylcholine (DPPC) lipids dispersed in $CaCl_2$ or $ZnCl_2$ solutions have been studied by SANS [84,86], and planar multilayers hydrated through water vapor by SAND [85]. The results confirm that both Ca^{2+} and Zn^{2+} cations bind to DPPC bilayers. This fact is reflected in the increased lamellar *d*-spacing that is most likely the result of charge-induced repulsion between

bilayers. This observation is consistent with other zwitterionic lipid multilayers, which swelled in the presence of $CaCl_2$ at 1–50 mM concentrations to the point that they became unbound (i.e., infinite *d*-spacing) [87–89]. In the case of vesicular systems, multilamellar DPPC dispersions convert completely into ULVs when the surface charge density is higher than 1–2 $\mu C/cm^2$ [90]. The initial swelling is most likely due to an increase in interbilayer electrostatic repulsion that is screened at high salt concentrations. Supposedly however, membrane structure is not affected at these high salt concentrations [91]. Interestingly, the low salt concentration results reveal that even the changes in internal structure (e.g., D_B and A_{UC} shown in Figure 1.11b and c) contribute to the increases in *d*-spacing. Moreover, Ca^{2+} and Zn^{2+} do not have the same effects.

Initially, both Ca^{2+} and Zn^{2+} cause DPPC bilayers to thicken, while further increases in Ca^{2+} concentration result in the bilayer thinning, eventually reverting to having the same thickness as pure DPPC. In the case of Zn^{2+} however, there is a typical binding isotherm behavior displayed by a monotonic increase of *d*-spacing and D_B, after which they both seem to plateau. The most pronounced difference is exhibited by D_B whose changes are compensated by the changes in interlamellar water spacing, resulting in a *d*-spacing that is practically unaffected by changes in cation concentration [85]. One can therefore disregard the effect that adjacent bilayers have on each other in the stacked system. This is supported also by the results, whereby ULVs dispersed in the water solution loaded with either Zn^{2+} or Ca^{2+} ions displayed similar trends in bilayer thickness changes. The data then imply that a small curvature present in the ULVs is not an important factor affecting the bilayer structure of ion containing DPPC membranes and that the effect of cations on bilayer thickness is the result of electrostatic interactions, rather than geometrical constraints due to bilayer curvature.

Finally, the experimental observations supported by MD simulations suggest differences in the binding specificity of Ca^{2+} and Zn^{2+} cations to lipid bilayers [85]. As confirmed by the radial distribution functions calculated from the simulations, both cations interact strongly with the negatively charged oxygen. However, the distributions also show that Ca^{2+} forms a contact pair with any headgroup atom much more favorably than Zn^{2+}. The differences between the structural changes experienced by DPPC bilayers when Ca^{2+} or Zn^{2+} is introduced may be rationalized well by the physical differences between the two cations. Calcium ions have a larger ionic radius (1 Å) than zinc ions (0.75 Å) [81]. In addition, the hydrogen bonding of water molecules extends beyond the ion's primary hydration shell – their crystal arrangements in bulk water have been proposed to be $Zn[H_2O]_6^{2+} \cdot [H_2O]_{12}$ and $Ca[H_2O]_{6.1}^{2+} \cdot [H_2O]_{5.29}$ [92, 93]. Calcium ions as a consequence of their larger size thus require smaller amounts of energy for the removal of hydration shell water. These observations imply that lipid–ion interactions do not only depend on which cation is present but also on their interactions with water, one of the smallest and often neglected biomolecules [94]. Apparently, Ca^{2+} ions create about 1.6 times fewer pairs with surrounding water molecules than do Zn^{2+} ions (Figure 12a), when interacting with DPPC bilayers. This smaller Ca^{2+} hydration shell most likely allows for more proximal and stronger contacts with the

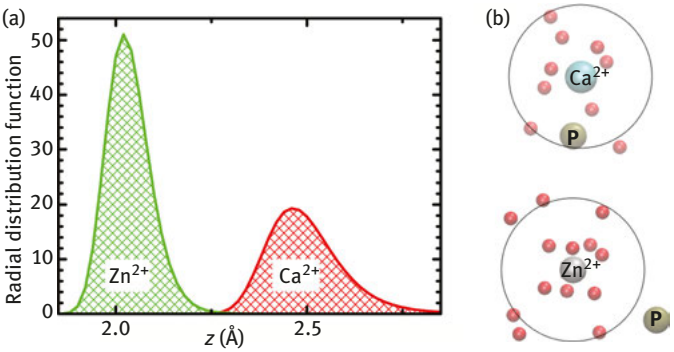

Figure 1.12: (**a**) Radial distribution functions for Zn^{2+}– and Ca^{2+}–water pairs determined from MD simulations. Areas under the peaks correspond to the number of water molecules present in the hydration shell of each cation interacting with the lipid bilayer (this number is smaller for Ca^{2+}, compared to Zn^{2+}). (**b**) Schematics of the hydration shells around Ca^{2+} (top) and Zn^{2+} (bottom) suggest fewer hydrating water molecules (red spheres) and closer proximity to the lipid's phosphate (P) in the case of Ca^{2+} cation. Results are adapted from Kučerka et al. [85].

lipid phosphate (see Figure 12b). Intriguingly, all of the mentioned interactions become increasingly important when functionalizing the model membrane systems with specific applications such as drug and/or gene delivery discussed in the following section.

1.6 Structural polymorphism of DNA–PC–Me^{2+} aggregates

Divalent metal cations play an important role as a mediator of many interactions: the binding or insertion of proteins to membranes, membrane fusion, transport of small molecules across membrane, etc. In addition to proteins, also the role of nucleic acid (NA)–lipid interactions in the functioning of cells and formation of a number of cellular structures became of great interest nowadays. For example, the role of NA–lipid–Me^{2+} in nuclear pore assembly [95, 96], signal transduction, and stimulation of DNA and RNA synthesis by endonuclear lipids [97], their presence in chromatin [98], or regulation of cell's lipid composition during cell division [99] received an attention in recent decades. There are many divalent metals of interest, including calcium and magnesium, iron, manganese, copper, zinc, nickel, and cobalt that are essential to life. On the other hand, they may become toxic beyond the level of appropriate concentration. We have shown different effect of calcium and zinc on DPPC bilayers in previous paragraph. Here, we illustrate differences in polymorphic behavior of aggregates formed due to DNA interactions with DPPC bilayers in the presence of Me^{2+}, while selecting Ca^{2+}

as typical earth metal, transition metal Co^{2+}, and Zn^{2+}. Intriguingly, the fluorescence experiments have confirmed the ability of Zn^{2+} to condense DNA in presence of lipid bilayer and to protect it against thermal denaturation up to the level comparable with Ca^{2+} and Mg^{2+} [100]. Cobalt is a trace element, integral part of vitamin B12, cobalamin, and it is involved in the production of erythropoietin, a hormone that stimulates the formation of erythrocytes. This property of cobalt was applied in the past as a therapy for anemia. On the other hand, Co^{2+} ions are genotoxic *in vitro* and *in vivo*, likely due to the involvement of oxidative stress and DNA repair inhibition, and they proved carcinogenic in rodents [101].

Generally, in a system DNA–phospholipid–divalent metal cations, one must consider the following binding events:

$$\mathrm{DNA} + \mathrm{PC} + \mathrm{Me}^{2+} \rightarrow \begin{cases} \mathrm{PC} + \mathrm{Me}^{2+} \\ \mathrm{DNA} + \mathrm{PC} + \mathrm{Me}^{2+} \\ \mathrm{DNA} + \mathrm{Me}^{2+} \end{cases}$$

Phospholipid–Me^{2+} interactions: Divalent metal cations bind naturally to negatively charged phospholipids [102, 103] but rather weakly to zwitterionic lipids as PC and PE [104, 105]. The binding mechanism of Me^{2+} on PC bilayers has been studied using many physicochemical methods. As a result of these studies, it is generally accepted that the preference for Me^{2+} binding weakens with an increasing degree of hydrocarbon chain unsaturation, and that it depends on the phospholipid phase (gel > fluid). Due to Me^{2+} binding, the negative charge of phosphate group of the $P–N^+$ dipole is neutralized and the lipid bilayer becomes positively charged. The electrostatic repulsion between bilayers makes them to swell in excess water up to the level promoting formation of ULVs, as discussed in the previous section. It should be mentioned that the phenomena of "unbound state," that is, spontaneous formation of ULVs, depends on experimental circumstances, such as temperature and concentrations of both lipid and Me^{2+}.

DNA–Me^{2+} interactions: DNA interacts readily with Me^{2+}, which may alter its structure inducing for example right-handed-to-left-handed helical transition [106], denaturation [107, 108], etc.; and thus, its function is modulated. Alkaline earth Me^{2+} (Ca^{2+}, Mg^{2+}) preferentially interacts with the phosphate groups of DNA, stabilizing the polynucleotide molecule [109]. Transition metal cations interact more extensively with DNA bases inducing disruption of base pairing, and destabilization of DNA [108, 109]. The affinity of Me^{2+} to DNA bases was reported to decrease in the order $Hg^{2+} > Cu^{2+} > Pb^{2+} > Cd^{2+} > Zn^{2+} > Mn^{2+} > Ni^{2+} > Co^{2+} > Fe^{2+} > Ca^{2+} > Mg^{2+}$, Ba^{2+} [110].

DNA–phospholipid–Me^{2+} interactions: Divalent metal cations mediate the interactions between DNA and PC bilayers, as has been shown four decades ago [111]. Microcalorimetry, turbidimetry, infrared spectroscopy, electron spin resonance spectroscopy, and other experimental methods were employed to characterize "a new phase" formed due to DNA interactions with PC vesicles in presence of Me^{2+} [112–116]. Electron freeze fracture micrographs of DNA–PCs–Ca^{2+} mixtures suggested structures with long-

range organization [117–119]. Finally, small-angle X-ray diffraction experiments have confirmed the ability of divalent cations to condense DNA into aggregates with internal long-range order of similar topology as it was found in complexes of DNA-cationic lipid studied extensively as nonviral delivery vectors for human gene therapy (Figure 1.13).

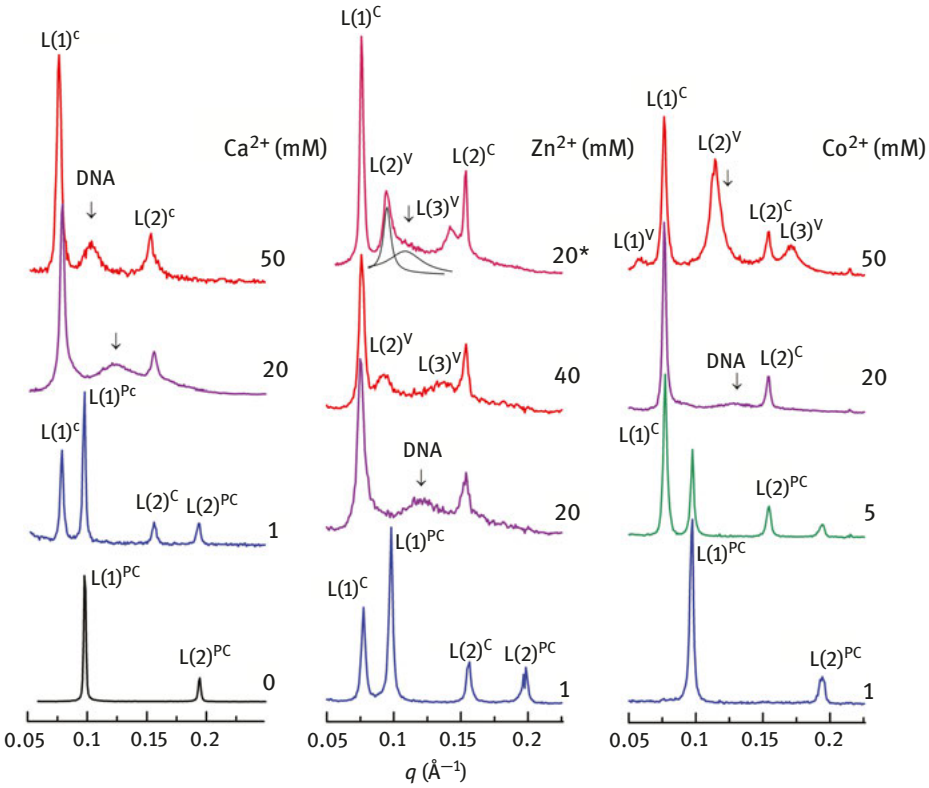

Figure 1.13: Small-angle X-ray diffraction (SAXD) curves of DNA–DPPC–Me^{2+} aggregates (DPPC:DNA = 3:1 mol/base) at selected concentrations of Me^{2+}, and at $T = 20$ °C. The total ionic strength in the diffractogram denoted by asterisk (*) was modulated with NaCl to $Is = 122$ mM.

For easier orientation in the structural polymorphism of aggregates, it is useful to introduce the lipid itself. Fully hydrated DPPC at 20 °C forms a lamellar phase (L) (Figure 1.13). Its temperature behavior is well characterized by a tilted gel phase ($L_{\beta'}$) below 35 °C, rippled gel phase (P_{β}) below 42 °C, and liquid-crystalline phase (L_{α}) above 42 °C [120].

About 1 mM solution of $CaCl_2$ or $ZnCl_2$ is sufficient for DNA complexation between DPPC bilayers (Figure 1.13). The diffractograms show the superposition of two one-

dimensional structures. Peaks $L(1)^{PC}$ and $L(2)^{PC}$ are attributed to a phase with a periodicity close to that formed by the lipid itself (d ~65 Å). The second lamellar phase with the repeat distance d ~80 Å is identified as a condensed L^C phase. This concentration of Me^{2+} (1 mM) is, however, not sufficient to facilitate regular packing of DNA strands; thus, we do not observe any peak related to DNA–DNA interhelical distance. Sketch of the structure is shown in Figure 1.14c. Such a coexistence of two lamellar phases is frequently reported in aggregates formed using both saturated or monounsaturated PC and DNA also at higher concentrations of Ca^{2+}, Mg^{2+}, and Mn^{2+} [121–124]. Note that the structure of DNA–DPPC in 1 mM solution of $CoCl_2$ is different. We observe only one lamellar phase with d ~65 Å that is comparable to DPPC itself. In this experiment, all samples were prepared at the same conditions. In the case of Co^{2+}, a solution with a higher concentration of salt is necessary for DNA complexation between lipid bilayers.

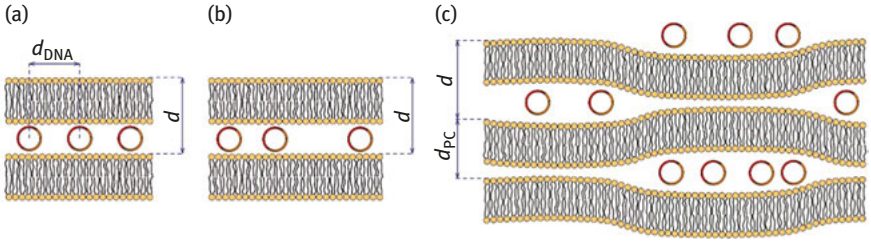

Figure 1.14: Schematic sketch of structures showing condensed lamellar phase (L^C) with (**a**) and without (**b**) regular DNA organization. The panel (**c**) shows a coexistence of two lamellar phases formed in consequence of lateral segregation of DNA strands (with permission Uhríková [125]).

About 20 mM of Me^{2+} (Ca^{2+}, Zn^{2+}, and Co^{2+}) is a sufficient concentration to induce a formation of condensed lamellar phase (L^C) with DNA strands packed regularly between DPPC bilayers in a gel state (T = 20 °C) (Figure 1.13). Two sharp peaks correspond to a lamellar phase with periodicity d ~80 Å, resulting from lipid bilayer stacking. The broad peak of lower intensity is an evidence for DNA–DNA organization. The interhelical DNA–DNA distance, d_{DNA} ~50–60 Å, is typical for DNA–DPPC–Me^{2+} aggregates in L_β^C phase with the lipid in a gel state [126, 127]. Similar diffractograms were observed for L^C phase in DNA–cationic lipid complexes [128, 129]. Figure 1.14a shows a schematic sketch of such L^C phase.

Finally, high concentrations of salts ($c_{Me}^{2+} \geq 40$ mM) affect aggregation process further and may change the structures. For example, we observe L_β^C phase with a well-defined DNA peak (d_{DNA} ~61 Å) as the only structure of DNA–DPPC–Ca^{2+} prepared at 50 mM of Ca^{2+} and at 20 °C. However, diffraction patterns of DNA–DPPC dispersed either in 40 mM of $ZnCl_2$ or 50 mM of $CoCl_2$ show systems with two phases. An analysis of the pattern with zinc revealed the coexistence of L_β^C phase with lattice

parameters d = 85 Å and d_{DNA} = 61 Å, and another lamellar phase, L^V, of a large periodicity d^V = 135 Å. Similar lattice parameters were extracted from diffractograms of DNA–DPPC in 50 mM of $CoCl_2$: L_β^C phase with d = 82 Å and d_{DNA} = 55 Å, and L^V phase with d^V = 109 Å. Since, the periodicity of L^V phase (~100–135 Å) is too big to be "accommodated" in a structure as shown in Figure 1.14c, this has indicated rather a destruction of the long-range lamellar structure of the lipid by its swelling into excess water, as discussed above for phospholipid–Me^{2+} interactions. In such a case, the periodicity is dictated by the total number of ions in solution (for DLVO theory, see, e.g., Ref. [130])

Further, we have therefore examined the effect of "a quantity" of ions. Figure 1.13 displays also the diffractogram of DNA–DPPC in 20 mM of $ZnCl_2$, where we modulated ionic strength (*Is*) by adding of NaCl (total ionic strength *Is* = 122 mM). The observed structural parameters (d = 82 Å, d_{DNA} = 57 Å, and d^V = 131 Å) are close to those found in previously discussed systems (i.e., DNA–DPPC in 40 mM $ZnCl_2$). It has been shown that neither the repeat distance nor the bilayer thickness of neutral phospholipids changed with the solution ionic strength ranging between 1 and 500 mM NaCl [131]. Figure 1.15 shows the effect of ionic strength on structural parameters of both detected phases, L^C and L^V. With increasing *Is*, we can see two opposite effects: the repeat distance d_L^C of condensed L^C phase formed by DNA–DPPC–Zn^{2+} increases slightly at $c_{Zn}^{2+} > 20$ mM (Figure 1.15, inset), and its total change does not exceed $\Delta d_L^C \sim 3$ Å. However, the repeat distance d_L^V of L^V phase decreases nonlinearly, changing significantly from ~200 Å to ~70 Å at *Is* = 330 mM, reaching almost the periodicity of pure DPPC (~64 Å). L^V phase was identified as being formed by DPPC + Zn^{2+} bilayers, and it is macroscopically separated from the mixture [132]. The mixture of DNA–DPPC–Co^{2+} at 50 mM of $CoCl_2$ has shown similar SAXD pattern. In addition to L^C phase formed by DNA condensed between DPPC and Co^{2+} bilayers, a part of the mixture is structured in a lamellar phase (L^V). Unfortunately, SAXD cannot discriminate between the coexistence of two phases that are, though macroscopically separated, both present within the studied volume of a sample or that coexist within one structure.

The driving force for mutual condensation of DNA by cationic vesicles to form an ordered, composite phase is the gain in electrostatic energy. The electrostatic energy depends on the surface charge densities of separated macroions, the structure and composition of the condensed phases, and the salt concentration in solution [133, 134]. The minima in electrostatic free energy occur when the fixed negative charges on DNA surface are balanced by the same number of positive charges on the bilayer surface, that is, at isoelectric point. Due to the high mobility of Me^{2+}, it is difficult to evaluate the isoelectric point in this system. The mechanism of DNA–phospholipid–Me^{2+} interactions and binding stoichiometry are still under discussion (see, e.g., Refs. [121, 124, 135]). DNA binding onto zwitterionic bilayers in presence of Me^{2+} is not driven by the release of counterions as it was confirmed for DNA–cationic/neutral lipid systems [136].

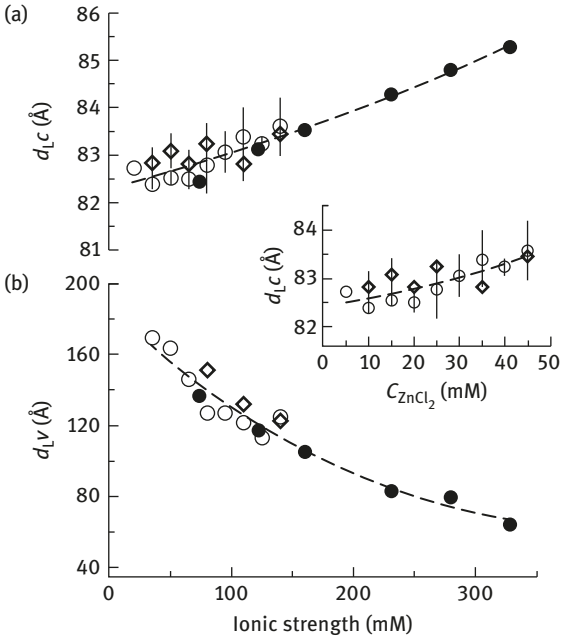

Figure 1.15: Dependence of the repeat distances *d* on the ionic strength (*Is*) of solutions (20 °C) for phases L^C (**a**) and L^V (**b**). The DNA–DPPC–Zn^{2+} aggregates were prepared either by DNA interacting with DPPC in solutions of Zn^{2+} at various concentrations (prepared in 5 mM of NaCl and represented by empty symbols) or $ZnCl_2$ was kept at constant concentration of 20 mM and ionic strength was modulated by NaCl (full symbols). The circles represent data from SANS, while the same samples measured by SAXD are shown by diamonds. **Inset**: the *d* of L^C as a function of $ZnCl_2$ concentration (c_{ZnCl_2}). Results are adapted from Uhríková et al. [132].

If salt is added to the system, the mobile salt ions screen electrostatic interactions between fixed charges along DNA and the $P–N^+$ dipole of phospholipid headgroups.

Structural polymorphism is reduced when the lipid is in a liquid-crystalline state (L_α phase). Figure 1.16a shows an evolution of structure with increasing temperature for DNA–DPPC–Ca^{2+} in 20 mM of Ca^{2+}. Note that the peak related to the DNA-DNA organization vanishes gradually into the background when the sample is heated, while it cannot be identified above ~60 °C. The analysis of the system reveals that the disorder in DNA lattice is caused mainly by in-plane fluctuations of DNA strands [126]. Due to the high mobility of metal cations, they do not induce constraints large enough to support DNA strands with the regular packing observed in complexes with cationic amphiphiles. Figure 1.16b illustrates temperature dependence of the repeat distance d_L^C for two different DNA–DPPC–Me^{2+} aggregates, prepared in 20 mM of Ca^{2+} and 40 mM of Co^{2+}, respectively. When comparing with pure DPPC, we see that DNA–DPPC–Me^{2+} aggregates show only one-phase transition: from gel to liquid-

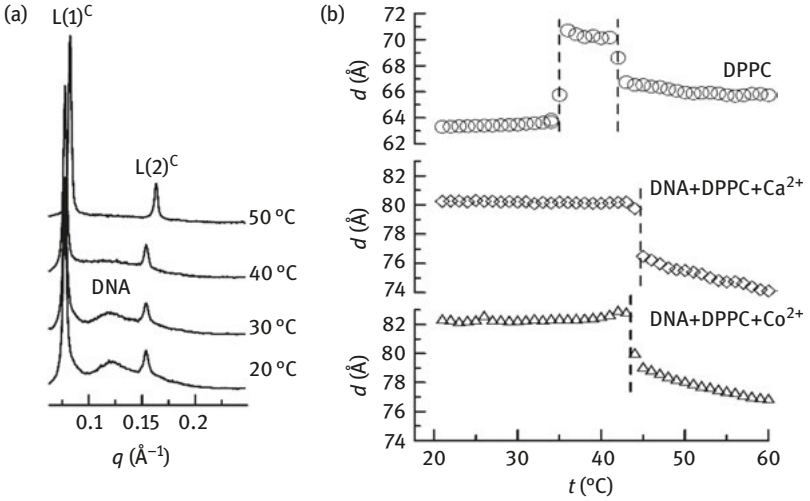

Figure 1.16: (**a**) SAX diffractograms of DPPC:DNA = 3:1 mol/base aggregates at 20 mM of Ca^{2+}. (**b**) Temperature dependences of the repeat distances (*d*) of fully hydrated DPPC bilayers and L^C phase of DNA–DPPC–Me^{2+} aggregates prepared at 20 mM of Ca^{2+} and 40 mM of Co^{2+}.

crystalline phase. DNA strands located in the water layer between bilayers dump the rippling of the DPPC bilayer, typically observed in the range 35–42 °C (P_β phase).

In a fluid lamellar L_α phase, a temperature increase induces an increase of the population of gauche conformers in lipid acyl chains accompanied by the lateral expansion of the bilayer, what is manifested by a decrease of the lipid thickness [137]. Indeed, Figure 1.16b shows d_L^C dropping by ~3–4 Å in the case of L^C phase due to DPPC acyl chains melting at $L_\beta^C \rightarrow L_\alpha^C$ phase transition. On the other hand, fluctuations of the lipid bilayer in L_α are enhanced, what is accompanied by a diffusion of water molecules from the bulk water phase in between lipid bilayers, thus an increase of the thickness of water layer [138]. The one of these two processes prevails the change in the repeat distance. As shown in Figure 1.16b, the repeat distances of both aggregates decrease with increasing temperature in L_α phase. In fact, DNA and Me^{2+} dump the bilayer fluctuations and make the bilayers "stiffer" showing higher resistance of lipid bilayers against water diffusion from the bulk aqueous phase [123]. The transversal thermal expansion coefficient at constant pressure π determined from

$$\alpha = \frac{1}{d}\left(\frac{\partial d}{\partial T}\right)_\pi,$$

where T is an absolute temperature and d is a suitable parameter to assess the system. For DPPC, we determined $\alpha = -(0.75 \pm 0.04) \times 10^{-3}\ K^{-1}$ by a linear least square fitting of

data in the range 50–60 °C. In triple complexes DNA–DPPC–Me^{2+} at 2–40 mM of Me^{2+}, and the same temperature range, α varies from about -1.6×10^{-3} to -2.1×10^{-3} K^{-1}. The α depends significantly on used Me^{2+}, decreasing in the order $\alpha_{DPPC} > \alpha_{Co^{2+}} > \alpha_{Ca^{2+}} \approx \alpha_{Zn^{2+}}$ [139].

The gel-to-liquid-crystalline phase transition of DPPC happens within the range T_{mDPPC} = 41.3 ± 1.8 °C, depending on the used experimental method [140]. Without Me^{2+}, DNA affects only slightly the thermodynamic parameters of DPPC [132]. On the other hand, DNA complexed with Me^{2+} affects phase transition of DPPC, as indicated in Figure 1.16b. Figure 1.17a summarizes changes to the DPPC's T_m detected in DNA–DPPC–Me^{2+} mixtures at different concentrations of cations using SAXD and differential scanning calorimetry (DSC). ΔT_m values expressed as $\Delta T_m = T_t - T_{mDPPC}$, where T_t is the phase transition temperature either of a condensed phase or a phase formed by DPPC + Me^{2+} in mixtures DNA–DPPC–Me^{2+} derived from both methods, are in a good accord. The effect of Me^{2+} on the melting of DPPC acyl chains bound in L^C phase of DNA–DPPC–Me^{2+} aggregates is evident, where T_m increases in the order: $T_{mDPPC} \approx T_{mCo} < T_{mCa} < T_{mZn}$. DSC profiles of DNA–DPPC–Zn^{2+} mixtures exhibit two well-defined maxima allowing to assess T_m and the enthalpy of both L^C phase of DNA–DPPC–Zn^{2+}, and L^{PC} phase of DPPC + Zn^{2+}. However, DSC does not distinguish between the lipid trapped in the DNA–DPPC–Zn^{2+} aggregate (L^{PC} phase) and that forming L^V phase (Figure 1.13), and thus, we use an abbreviation PC (L^{PC}). The effect of Zn^{2+} on DPPC phase transition without any DNA determined independently is shown in Figure 1.17a as well. In addition to T_m, the enthalpy (ΔH) of transition can be

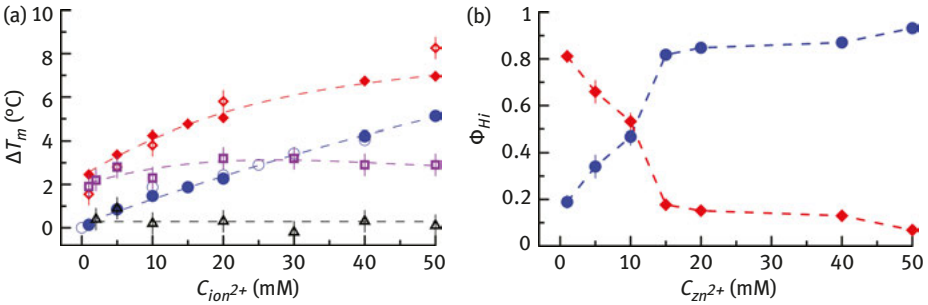

Figure 1.17: (**a**) Difference between the gel–liquid-crystal phase transition of DPPC (T_{mDPPC}) and that of DNA–DPPC–Me^{2+} as a function of Me^{2+} concentration ($\Delta T_m = T_t - T_{mDPPC}$). The ΔT_m for L^C phase of DNA–DPPC–Co^{2+} is displayed by empty triangles, L^C phase of DNA–DPPC–Ca^{2+} by empty squares, and L^C phase of DNA–DPPC–Zn^{2+} by empty diamonds. Data are derived from the discontinuities of repeat distance d of L^C phase in DNA–DPPC–Me^{2+} aggregates extracted from SAXD data [139]. The complementary data obtained from DSC are shown in the case of DNA–DPPC–Zn^{2+} mixture for L^C phase (full diamonds), L^{PC} phase (full circles), and for DPPC + Zn^{2+} mixture (empty circles). (**b**) The enthalpy fraction Φ_{H_i} of individual phases L_i (i = PC, C) versus $ZnCl_2$ concentration. The results are adapted from Uhríková et al. [132].

calculated by integrating the heat capacity versus temperature curve of DSC profile. In order to quantify the relative changes in the volume fraction of individual phases, we express the enthalpy fraction Φ_{H_i}:

$$\Phi_{H_i} = \frac{\Delta H_i}{\Delta H_{\text{tot}}},$$

where ΔH_i is the enthalpy of $i = L^C$, L^{PC} phases and ΔH_{tot} is the total enthalpy. The ΔH_i of ith phase as well as the total enthalpy were determined by integration of the calorimetric profile [132]. Relative changes in the enthalpy of individual phases as a function of $ZnCl_2$ concentration are depicted in Figure 1.17b. Note the pronounced changes in the volume fractions of both phases at low concentrations of Zn^{2+} (<20 mM). Volume fraction of lipid involved in the condensed lamellar phase with DNA (L^C phase) decreases significantly with increasing concentration of zinc. High content of the salt has an influence on thermal stability. For example, aggregates prepared with short fragmented DNA in 20 mM of $ZnCl_2$ have lost their long-range order when heated to 60 °C [132]. We did not detect such behavior in aggregates prepared with highly polymerized DNA. As mentioned above, both cations Zn^{2+} and Co^{2+} have shown good affinity for DNA bases. In solutions with higher concentrations of these Me^{2+}, binding sites of both DNA and DPPC are saturated, and cations do not mediate the binding any more. The electrostatic screening of Me^{2+} charge due to ion accumulation and formation of a diffuse double layer at the lipid bilayer surface then leads to a macroscopic phase separation.

To conclude, DNA–phospholipid–Me^{2+} aggregates show higher structural varieties in comparison to complexes of DNA-cationic liposomes prepared with cationic lipid or surfactant. Divalent cations are active in promoting DNA condensation into the ternary complexes. As we demonstrated shortly, using one phospholipid (DPPC) and three cations of Me^{2+} (Ca^{2+}, Zn^{2+}, and Co^{2+}) modified thermodynamic properties and polymorphic behavior of ternary complexes. An attenuation of DNA binding in solutions at higher ionic strength appears as a drawback for their consideration as gene carriers in human therapy. On the other hand, the toxicity of metals results from the formation of complexes with organic compounds. The knowledge of the structure and phase behavior of the formed aggregates can thus contribute to the understanding of their toxicity.

Acknowledgments

The authors thank S.S. Funari for his assistance with SAXD experiments, and A. Lengyel for providing selected data from his PhD thesis. Financial support provided by the EC Program (FP7/2007–2013) under grant agreement no. 226716 (HASYLAB project II-20100372 EC), by the JINR topical theme 04-4-1121-2015/2020, by the CENI/ILL agreement 2014-2018, and by grant VEGA 1/0916/16 is gratefully acknowledged.

References

[1] Gorter, E., & Grendel, F. On bimolecular layers of lipoids on the chromocytes of the blood. J. Exp. Med. 1925, 41, 439–443.

[2] Danielli, J.F., & Davson, H. A contribution to the theory of permeability of thin films. J. Cell. Comp. Physiol. 1935, 5, 495–508.

[3] Singer, S.J., & Nicolson, G.L. The fluid mosaic model of the structure of cell membranes. Science. 1972, 175, 720–731.

[4] Nicolson, G.L. The fluid-mosaic model of membrane structure: still relevant to understanding the structure, function and dynamics of biological membranes after more than 40 years. Biochim. Biophys. Acta. 2014, 1838, 1451–1466.

[5] Engelman, D.M. Membranes are more mosaic than fluid. Nature. 2005, 438, 578–580.

[6] Simons, K., & Ikonen, E. Functional rafts in cell membranes. Nature. 1997, 387, 569–572.

[7] Escriba, P.V., Gonzalez-Ros, J.M., Goni, F.M., et al. Membranes: a meeting point for lipids, proteins and therapies. J. Cell. Mol. Med. 2008, 12, 829–875.

[8] van Meer, G., Voelker, D.R., & Feigenson, G.W. Membrane lipids: where they are and how they behave. Nat. Rev. Mol. Cell. Biol. 2008, 9, 112–124.

[9] Cullis, P.R., & Hope, M.J. Physical properties and structural roles of lipids in membranes. In: D.E. Vance & J.E. Vance, eds. Biochemistry of Lipids and Membranes: The Benjamin/Cumings Publishing Company, Don Mills, Ontario. Inc.; 1985, 25–72.

[10] Tanford, C. The Hydrophobic Effect: Formation of Micelles and Biological Membranes. Second Edition ed. New York: John Wiley and sons; 1980.

[11] Cevc, G., & Marsh, D. Phospholipid Bilayers. Physical Principles and Models. New York: John Wiley & Sons, Inc.; 1987, 157–231.

[12] Yeagle, P. The structure of biological membranes. Boca Raton: CRC Press; 1992. Second Ed. 2005, 201–241.

[13] Kučerka, N., Heberle, F.A., Pan, J., & Katsaras, J. Structural significance of lipid diversity as studied by small angle neutron and X-ray scattering. Membranes (Basel). 2015, 5, 454–472.

[14] Weijers, R.N. Lipid composition of cell membranes and its relevance in type 2 diabetes mellitus. Curr. Diabetes Rev. 2012, 8, 390–400.

[15] Katsaras, J., Pencer, J., Nieh, M.P., Abraham, T., Kučerka, N., & Harroun, T.A. Neutron and X-Ray Scattering from Isotropic and Aligned Membranes. Structure and Dynamics of Membranous Interfaces: John Wiley & Sons, Hoboken, New Jersey. Inc. 2008, 107–134.

[16] Harroun, T.A., Kučerka, N., Nieh, M.P., & Katsaras, J. Neutron and X-ray scattering for biophysics and biotechnology: examples of self-assembled lipid systems. Soft Matter. 2009, 5, 2694–2703.

[17] Heberle, F.A., Pan, J., Standaert, R.F., Drazba, P., Kučerka, N., & Katsaras, J. Model-based approaches for the determination of lipid bilayer structure from small-angle neutron and X-ray scattering data. Eur. Biophys. J. 2012, 41, 875–890.

[18] Wiener, M.C., & White, S.H. Fluid bilayer structure determination by the combined use of x-ray and neutron diffraction. I. fluid bilayer models and the limits of resolution. Biophys. J. 1991, 59,162–173.

[19] Kučerka, N., Nagle, J.F., Sachs, J.N., et al. Lipid bilayer structure determined by the simultaneous analysis of neutron and X-ray scattering data. Biophys. J. 2008, 95, 2356–2367.

[20] Nagle, J.F., & Tristram-Nagle, S. Structure of lipid bilayers. Biochim. Biophys. Acta. 2000, 1469, 159–195.

[21] Nagle, J.F., Zhang, R., Tristram-Nagle, S., Sun, W., Petrache, H.I., & Suter, R.M. X-ray structure determination of fully hydrated L alpha phase dipalmitoylphosphatidylcholine bilayers. Biophys. J. 1996, 70, 1419–1431.
[22] Balgavý, P., & Devínsky, F. Cut-off effects in biological activities of surfactants. Adv. Colloid. Interface Sci. 1996, 66, 23–63.
[23] Wassenaar, T.A., Ingolfsson, H.I., Bockmann, R.A., Tieleman, D.P., & Marrink, S.J. Computational lipidomics with insane: A versatile tool for generating custom membranes for molecular simulations. J. Chem. Theory Comput. 2015, 11, 2144–2155.
[24] Kučerka, N., Gallová, J., Uhríková, D., et al. Areas of monounsaturated diacylphosphatidylcholines. Biophys. J. 2009, 97, 1926–1932.
[25] Cornell, B.A., & Separovic, F. Membrane thickness and acyl chain length. Biochim. Biophys. Acta. 1983, 733,189–193.
[26] Kučerka, N., Nieh, M.P., & Katsaras, J. Fluid phase lipid areas and bilayer thicknesses of commonly used phosphatidylcholines as a function of temperature. Biochim. Biophys. Acta. 2011, 1808, 2761–2771.
[27] Karlovská, J., Uhríková, D., Kučerka, N., et al. Influence of N-dodecyl-N,N-dimethylamine N-oxide on the activity of sarcoplasmic reticulum Ca(2+)-transporting ATPase reconstituted into diacylphosphatidylcholine vesicles: effects of bilayer physical parameters. Biophys. Chem. 2006, 119, 69–77.
[28] Martinez-Seara, H., Rog, T., Pasenkiewicz-Gierula, M., Vattulainen, I., Karttunen, M., & Reigada, R. Effect of double bond position on lipid bilayer properties: insight through atomistic simulations. J. Phys. Chem. B. 2007, 111, 11162–11168.
[29] Petrache, H.I., Dodd, S.W., & Brown, M.F. Area per lipid and acyl length distributions in fluid phosphatidylcholines determined by (2)H NMR spectroscopy. Biophys. J. 2000, 79, 3172–3192.
[30] Shoemaker, S.D., & Vanderlick, T.K. Intramembrane electrostatic interactions destabilize lipid vesicles. Biophys. J. 2002, 83, 2007–2014.
[31] de Vrije, T., de Swart, R.L., Dowhan, W., Tommassen, J., & de Kruijff, B. Phosphatidylglycerol is involved in protein translocation across Escherichia coli inner membranes. Nature. 1988, 334, 173–175.
[32] Nikaido, H., & Vaara, M. Molecular basis of bacterial outer membrane permeability. Microbiol. Rev. 1985, 49, 1–32.
[33] Seddon, A.M., Lorch, M., Ces, O., Templer, R.H., Macrae, F., & Booth, P. J. Phosphatidylglycerol lipids enhance folding of an alpha helical membrane protein. J. Mol. Biol. 2008, 380, 548–556.
[34] Tristram-Nagle, S., Zhang, R., Suter, R.M., Worthington, C.R., Sun, W.J., & Nagle, J.F. Measurement of chain tilt angle in fully hydrated bilayers of gel phase lecithins. Biophys. J. 1993, 64, 1097–1109.
[35] McIntosh, T.J., & Simon, S.A. Area per molecule and distribution of water in fully hydrated dilauroylphosphatidylethanolamine bilayers. Biochemistry. 1986, 25, 4948–4952.
[36] Cantor, R.S. Lateral pressures in cell membranes: A mechanism for modulation of protein function. J. Phys. Chem. B. 1997, 101, 1723–1725.
[37] Marsh, D. Lateral pressure in membranes. Biochim. Biophys. Acta. 1996, 1286, 183–223.
[38] Marrink, S.J., de Vries, A.H., Harroun, T.A., Katsaras, J., & Wassall, S.R. Cholesterol shows preference for the interior of polyunsaturated lipid membranes. J. Am. Chem. Soc. 2008, 130, 10–11.
[39] Kučerka, N., Perlmutter, J.D., Pan, J., Tristram-Nagle, S., Katsaras, J., & Sachs, J.N. The effect of cholesterol on short- and long-chain monounsaturated lipid bilayers as determined by molecular dynamics simulations and X-ray scattering. Biophys. J. 2008, 95, 2792–2805.
[40] Harroun, T.A., Katsaras, J., & Wassall, S.R. Cholesterol hydroxyl group is found to reside in the center of a polyunsaturated lipid membrane. Biochemistry. 2006, 45, 1227–1233.

[41] Harroun, T.A., Katsaras, J., & Wassall, S.R. Cholesterol is found to reside in the center of a polyunsaturated lipid membrane. Biochemistry. 2008, 47, 7090–7096.
[42] Kučerka, N., Marquardt, D., Harroun, T.A., Nieh, M.P., Wassall, S.R., & Katsaras, J. The functional significance of lipid diversity: orientation of cholesterol in bilayers is determined by lipid species. J. Am. Chem. Soc. 2009, 131, 16358–16359.
[43] Katsaras, J., Kučerka, N., & Nieh, M.P. Structure from substrate supported lipid bilayers (Review). Biointerphases. 2008, 3, FB55.
[44] Wiener, MC, King, GI, & White, SH. Structure of a fluid dioleoylphosphatidylcholine bilayer determined by joint refinement of x-ray and neutron diffraction data. I. scaling of neutron data and the distributions of double bonds and water. Biophys. J. 1991, 60,568–576.
[45] Kučerka, N., Marquardt, D., Harroun, T.A., et al. Cholesterol in bilayers with PUFA chains: doping with DMPC or POPC results in sterol reorientation and membrane-domain formation. Biochemistry. 2010, 49, 7485–7493.
[46] Cornelius, F. Modulation of Na,K-ATPase and Na-ATPase activity by phospholipids and cholesterol. I. Steady-State kinetics. Biochemistry. 2001, 40, 8842–8851.
[47] Lee, A.G. Ca2+ -ATPase structure in the E1 and E2 conformations: mechanism, helix-helix and helix-lipid interactions. Biochim. Biophys. Acta. 2002, 1565, 246–266.
[48] Pencer, J., Krueger, S., Adams, C.P., & Katsaras, J. Method of separated form factors for polydisperse vesicles. J. Appl. Crystallogr. 2006, 39, 293–303.
[49] Kučerka, N., Nagle, J.F., Feller, S.E., & Balgavý, P. Models to analyze small-angle neutron scattering from unilamellar lipid vesicles. Phys. Rev. E. Stat. Nonlin. Soft Matter Phys. 2004, 69, 051903.
[50] Kučerka, N., Pencer, J., Nieh, M.P., & Katsaras, J. Influence of cholesterol on the bilayer properties of monounsaturated phosphatidylcholine unilamellar vesicles. Eur. Phys. J.E. 2007, 23, 247–254.
[51] Brzustowicz, M.R., & Brunger, A.T. X-ray scattering from unilamellar lipid vesicles. J. Appl. Cryst. 2005, 38, 126–131.
[52] Kučerka, N., Pencer, J., Sachs, J.N., Nagle, J.F., & Katsaras, J. Curvature effect on the structure of phospholipid bilayers. Langmuir. 2007, 23, 1292–1299.
[53] Kučerka, N., Nieh, M.P., & Katsaras, J. Asymmetric distribution of cholesterol in unilamellar vesicles of monounsaturated phospholipids. Langmuir. 2009, 25, 13522–13527.
[54] Friedman, R., Pellarin, R., & Caflisch, A. Amyloid aggregation on lipid bilayers and its impact on membrane permeability. J. Mol. Biol. 2009, 387, 407–415.
[55] Gellermann, G.P., Appel, T.R., Tannert, A., et al. Raft lipids as common components of human extracellular amyloid fibrils. Proc. Natl. Acad. Sci. U S A. 2005, 102, 6297–6302.
[56] Puglielli, L., Tanzi, R.E., & Kovacs, D.M. Alzheimer's disease: the cholesterol connection. Nature Neuroscience. 2003, 6, 345–351.
[57] Di Paolo, G., & Kim, T.W. Linking lipids to Alzheimer's disease: cholesterol and beyond. Nat. Rev. Neurosci. 2011, 12, 284–296.
[58] Benloucif, S., Burgess, H.J., Klerman, E.B., et al. Measuring melatonin in humans. J. Clin. Sleep. Med. 2008, 4, 66–69.
[59] Karasek, M. Melatonin, human aging, and age-related diseases. Exp. Gerontol. 2004, 39, 1723–1729.
[60] Olcese, J.M., Cao, C., Mori, T., et al. Protection against cognitive deficits and markers of neurodegeneration by long-term oral administration of melatonin in a transgenic model of Alzheimer disease. J. Pineal. Res. 2009, 47, 82–96.
[61] Severcan, F., Sahin, I., & Kazanci, N. Melatonin strongly interacts with zwitterionic model membranes--evidence from Fourier transform infrared spectroscopy and differential scanning calorimetry. Biochim. Biophys. Acta. 2005, 1668, 215–222.

[62] Garcia, J.J., Reiter, R.J., Guerrero, J.M., et al. Melatonin prevents changes in microsomal membrane fluidity during induced lipid peroxidation. FEBS. Lett. 1997, 408, 297–300.
[63] Saija, A., Tomaino, A., Trombetta, D., et al. Interaction of melatonin with model membranes and possible implications in its photoprotective activity. Eur. J. Pharm. Biopharm. 2002, 53, 209–215.
[64] de Lima, V.R., Caro, M.S., Munford, M.L., et al. Influence of melatonin on the order of phosphatidylcholine-based membranes. J. Pineal. Res. 2010, 49, 169–175.
[65] Bongiorno, D., Ceraulo, L., Ferrugia, M., Filizzola, F., Ruggirello, A., & Liveri, V.T. Localization and interactions of melatonin in dry cholesterol/lecithin mixed reversed micelles used as cell membrane models.J. Pineal. Res. 2005, 38, 292–298.
[66] Rosales-Corral, S.A., Acuna-Castroviejo, D., Coto-Montes, A., et al. Alzheimer's disease: pathological mechanisms and the beneficial role of melatonin. J. Pineal. Res. 2012, 52, 167–202.
[67] Pabst, G., Kučerka, N., Nieh, M.P., Rheinstädter, M.C., & Katsaras, J. Applications of neutron and X-ray scattering to the study of biologically relevant model membranes. Chem. Phys. Lipids. 2010, 163, 460–479.
[68] Kučerka, N., Nieh, M.P., Pencer, J., Sachs, J.N., & Katsaras, J. What determines the thickness of a biological membrane. Gen. Physiol. Biophys. 2009, 28, 117–125.
[69] Worcester, D.L., & Franks, N.P. Structural analysis of hydrated egg lecithin and cholesterol bilayers. II. Neutrol diffraction. J. Mol. Biol. 1976, 100, 359–378.
[70] Leonard, A., Escrive, C., Laguerre, M., et al. Location of cholesterol in DMPC membranes. A comparative study by neutron diffraction and molecular mechanics simulation. Langmuir. 2001, 17, 2019–2030.
[71] Drolle, E., Kučerka, N., Hoopes, M.I., et al. Effect of melatonin and cholesterol on the structure of DOPC and DPPC membranes. Biochim. Biophys. Acta. 2013, 1828, 2247–2254.
[72] Sack, R.L., Lewy, A.J., Erb, D.L., Vollmer, W.M., & Singer, C.M. Human melatonin production decreases with age. J. Pineal. Res. 1986, 3, 379–388.
[73] Robinson, D.H., & Toledo, A.H. Historical development of modern anesthesia. J. Invest. Surg. 2012, 25, 141–149.
[74] Mullins, L.J. Some Physical Mechanisms in Narcosis. Chem. Rev. 1954, 54, 289–323.
[75] Lee, A.G. Model for action of local anaesthetics. Nature. 1976, 262, 545–548.
[76] Franks, N.P., & Lieb, W.R. Molecular mechanisms of general anaesthesia. Nature. 1982, 300, 487–493.
[77] Heimburg, T., & Jackson, A.D. The thermodynamics of general anesthesia. Biophys. J. 2007, 92, 3159-65.
[78] Graesboll, K., Sasse-Middelhoff, H., & Heimburg, T. The thermodynamics of general and local anesthesia. Biophys. J. 2014, 106, 2143–2156.
[79] Kondela, T., Gallová, J., Hauß, T., Barnoud, J., Marrink, S.J., & Kučerka, N. Alcohol Interactions with Lipid Bilayers. Molecules. 2017, 22, 2078.
[80] Chu, N., Kučerka, N., Liu, Y., Tristram-Nagle, S., & Nagle, J.F. Anomalous swelling of lipid bilayer stacks is caused by softening of the bending modulus. Phys. Rev. E. Stat. Nonlin. Soft Matter Phys. 2005, 71, 041904.
[81] Binder, H., & Zschornig, O. The effect of metal cations on the phase behavior and hydration characteristics of phospholipid membranes. Chem. Phys. Lipids. 2002, 115, 39–61.
[82] Kučerka, N., Papp-Szabo, E., Nieh, M.P., et al. Effect of cations on the structure of bilayers formed by lipopolysaccharides isolated from Pseudomonas aeruginosa PAO1. J. Phys. Chem. B. 2008, 112, 8057–8062.

[83] Abraham, T., Schooling, S.R., Nieh, M.P., Kučerka, N., Beveridge, T.J., & Katsaras, J. Neutron diffraction study of Pseudomonas aeruginosa lipopolysaccharide bilayers. J. Phys. Chem. B. 2007, 111, 2477–2483.
[84] Uhríková, D., Kučerka, N., Lengyel, A., et al. Lipid bilayer – DNA interaction mediated by divalent metal cations: SANS and SAXD study. J. Phys.: ConferenceSeries. 2012, 351, 012011-1-9.
[85] Kučerka, N., Dushanov, E., Kholmurodov, K.T., Katsaras, J., & Uhríková, D. Calcium and zinc differentially affect the structure of lipid membranes. Langmuir. 2017, 33, 3134–3141.
[86] Uhríková, D., Kučerka, N., Teixeira, J., Gordeliy, V., & Balgavý, P. Structural changes in dipalmitoylphosphatidylcholine bilayer promoted by Ca2+ ions: a small-angle neutron scattering study. Chem. Phys. Lipids. 2008, 155, 80–89.
[87] Yamada, L., Seto, H., Takeda, T., Nagao, M., Kawabata, Y., & Inoue, K. SAXS, SANS and NSE studies on "Unbound State" in DPPC/Water/CaCl2 system. J. Phys. Soc. Jpn. 2005, 74, 2853–2859.
[88] Inoko, Y., Yamaguchi, T., Furuya, K., & Mitsui, T. Effects of cations on dipalmitoyl phosphatidylcholine/cholesterol/water systems. Biochim. Biophys. Acta. 1975, 413, 24–32.
[89] Uhríková, D., Teixeira, J., Lengyel, A., Almasy, L., & Balgavý, P. Formation of unilamellar dipalmitoylphosphatidylcholine vesicles promoted by Ca2+ ions: A small-angle neutron scattering study. Spectrosc.-An Int. J. 2007, 21, 43–52.
[90] Hauser, H. Phospholipid Vesicles. In: G. Cevc, ed. Phospholipid Handbook. New York: Marcel Dekker, Inc. 1993:603–637.
[91] Petrache, H.I., Tristram-Nagle, S., Harries, D., Kučerka, N., Nagle, J.F., & Parsegian, V.A. Swelling of phospholipids by monovalent salt. J. Lipid. Res. 2006, 47, 302–309.
[92] Bock, C.W., Markham, G.D., Katz, A.K., & Glusker, J.P. The arrangement of first- and second-shell water molecules in trivalent aluminum complexes: results from density functional theory and structural crystallography. Inorg. Chem. 2003, 42, 1538–1548.
[93] David, F., Vokhmin, V., & Ionova, G. Water characteristics depend on the ionic environment. Thermodynamics and modelisation of the aquo ions. J. Mol. Liquids. 2001, 90, 45–62.
[94] Chaplin, M. Do we underestimate the importance of water in cell biology?. Nat. Rev. Mol. Cell Biol. 2006, 7, 861–866.
[95] Kuvichkin, V.V. DNA-lipid interactions in vitro and in vivo. Bioelectrochemistry. 2002, 58, 3–12.
[96] Kuvichkin, V.V. The mechanism of a nuclear pore assembly: A molecular biophysics view. J. Membrane. Biol. 2011, 241, 109–116.
[97] Martelli, A.M., Fala, F., Faenza, I., et al. Metabolism and signaling activities of nuclear lipids. Cell Mol. Life Sci. 2004, 61, 1143–1156.
[98] Albi, E., Lazzarini, R., & Viola Magni, M. Phosphatidylcholine/sphingomyelin metabolism crosstalk inside the nucleus. Biochem. J, 2008, 410, 381–389.
[99] Atilla-Gokcumen, G.E., Muro, E., Relat-Goberna, J., et al. Dividing cells regulate their lipid composition and localization. Cell. 2014, 156, 428–439.
[100] Lengyel, A., Uhríková, D., Klacsová, M., & Balgavý, P. DNA condensation and its thermal stability influenced by phospholipid bilayer and divalent cations. Colloids. Surf. B. 2011, 86, 212–217.
[101] De Boeck, M., Kirsch-Volders, M., & Lison, D. Cobalt and antimony: genotoxicity and carcinogenicity. Mutat Res. 2003, 533, 135–152.
[102] Macdonald, P.M., & Seelig, J. Calcium binding to mixed phosphatidylglycerol-phosphatidylcholine bilayers as studied by deuterium nuclear magnetic resonance. Biochemistry. 1987, 26, 1231–1240.
[103] Sinn, C.G., Antonietti, M., & Dimova, R. Binding of calcium to phosphatidylcholine-phosphatidylserine membranes. Colloids Surf. A-Physicochemical and Engineering Aspects. 2006, 282, 410–419.

[104] Altenbach, C., & Seelig, J. Ca2+ binding to phosphatidylcholine bilayers as studied by deuterium magnetic resonance. Evidence for the formation of a Ca2+ complex with two phospholipid molecules. Biochemistry. 1984, 23, 3913–3920.
[105] Satoh, K. Determination of binding constants of Ca^{2+}, Na^{+}, and Cl^{-} ions to liposomal membranes of dipalmitoylphosphatidylcholine at gel phase by particle electrophoresis. Biochim. Biophys. Acta. 1995, 1239, 239–248.
[106] Jovin, T.M., Soumpasis, D.M., & McIntosh, L.P. The transition between B-DNA and Z-DNA. Annu. Rev. Phys. Chem. 1987, 38, 521–560.
[107] Dove, W.F., & Davidson, N. Cation effects on the denaturation of DNA. J. Mol. Biol. 1962, 5, 467–478.
[108] Eichhorn, G.L., & Shin, Y.A. Interaction of metal ions with polynucleotides and related compounds. XII. the relative effect of various metal ions on DNA helicity. J. Am. Chem. Soc. 1968, 90, 7323–7328.
[109] Luck, G., & Zimmer, C. Conformational aspects and reactivity of DNA. effects of manganese and magnesium ions on interaction with DNA. Eur. J. Biochem. 1972, 29, 528–536.
[110] Duguid, J., Bloomfield, V.A., Benevides, J., & Thomas Jr., G.J. Raman spectroscopy of DNA-metal complexes. I. Interactions and conformational effects of the divalent cations: Mg, Ca, Sr, Ba, Mn, Co, Ni, Cu, Pd, and Cd. Biophys. J. 1993, 65, 1916–1928.
[111] Budker, V.G., Kazatchkov, Y.A., & Naumova, L.P. Polynucleotides adsorb on mitochondrial and model lipid membranes in the presence of bivalent cations. FEBS. Letters. 1978, 95, 143–146.
[112] Vojčíková, L., & Balgavý, P. Interaction of DNA with dipalmitoylphosphatidylcholine model membranes: A microcalorimetric study. Studia. Biophysica. 1988, 125, 5–10.
[113] Vojčíková, L., Švajdlenka, E., & Balgavý, P. Spin label and microcalorimetric studies of the interaction of DNA with unilamellar phosphatidylcholine liposomes. Gen. Physiol. Biophys. 1989, 8, 399–406.
[114] Balgavý, P., Vojčíková, L., & Švajdlenka, E. Microcalorimetric study the DNA melting in the presence of phosphatidylcholine liposomes and magnesium ions. Acta Facultatis Pharm. Univ. Comenianae. 2002, 49, 17–25.
[115] Bruni, P., Gobbi, G., Morganti, G., Iacussi, M., Maurelli, E., & Tosi, G. Use and activity of metals in biological systems. I. The interaction of bivalent metal cations with double-stranded polynucleotides and phospholipids. Gazz. Chim. Ital. 1997, 127, 513–517.
[116] Bruni, P., Cingolani, F., Iacussi, M., Pierfederici, F., & Tosi, G. The effect of bivalent metal ions on complexes DNA-liposome: a FT-IR study. J. Mol. Struc. 2001, 565–566.
[117] Tarahovsky, Y.S., Khusainova, A.V., Gorelov, A.V., et al. DNA initiates polymorphic structural transitions in lecithin. FEBS. Letters. 1996, 390, 133–136.
[118] Tarahovsky, Y.S., Deev, A.A., Masulis, I.S., & Ivanitsky, G.R. Structural organization and phase behavior of DNA-calcium- dipalmitoylphosphatidylcholine complex. Biochemistry-Moscow 1998, 63, 1126–1131.
[119] Khusainova, R.S., Dawson, K.A., Rochev, I., Gorelov, A.V., & Ivanitskii, G.R. Structural changes in DNA-Ca2+-dipalmitoylphosphatidylcholine complexes during changes in the molar ratio of nucleotide/lipid. Microcalorimetric study. Dokl. Akad. Nauk. 1999, 367, 553–556.
[120] Stumpel, J., Eibl, H.J., & Nicksch, A. X-ray analysis and calorimetry on phosphatidylcholine model membranes. Biochim. Biophys. Acta. 1983, 727, 246–254.
[121] McManus, J., Radler, J.O., & Dawson, K.A. Phase behaviour of DPPC in a DNA-calcium-zwitterionic lipid complex studied by small angle x-ray scattering. Langmuir. 2003, 19, 9630–9637.
[122] Francescangeli, O., Stanic, V., Gobbi, L., et al. Structure of self-assembled liposome-DNA-metal complexes. Phys. Rev. e. 2003, 67, art-011904.

[123] Uhríková, D., Hanulová, M., Funari, S.S., Khusainova, R.S., Šeršeň, F., & Balgavý, P. The structure of DNA–DOPC aggregates formed in presence of calcium and magnesium ions: a small angle synchrotron X ray diffraction study. Biochim. Biophys. Acta. 2005, 1713, 15–28.
[124] Bruni, P., Francescangeli, O., Marini, M., Mobbili, G., Pisani, M., & Smorlesi, A. Can neutral liposomes be considered as genetic material carriers for human gene therapy?. Mini-Rev. Org Chem. 2011, 8, 38–48.
[125] Uhríková, D. Divalent Metal Cations in DNA–Phospholipid Binding. In: A. Iglič & C.V. Kulkarni, eds. Advances in Planar Lipid Bilayers and Liposomes, vol 20. Burlington: Elsevier 2014:111–135.
[126] Uhríková, D., Lengyel, A., Hanulová, M., Funari, S.S., & Balgavý, P. The structural diversity of DNA-neutral phospholipids-divalent metal cations aggregates: a small-angle synchrotron X-ray diffraction study. Eur. Biophys. J. 2007, 36, 363–375.
[127] Uhríková, D., Rapp, G., & Balgavý, P. Condensation of DNA and phosphatidylcholine bilayers induced by Mg(II) ions – a synchrotron X-ray diffraction study. In: M. Melník & A. Sirota, eds. Challenges for Coordination Chemistry in the new Century. Bratislava: Slovak Technical University Press; 2001, 219–224.
[128] Lasic, D.D., Strey, H., Stuart, M.C.A., Podgornik, R., & Frederik, P.M. The structure of DNA-Liposome complexes. J. Am. Chem. Soc. 1997, 119, 832–833.
[129] Radler, J.O., Koltover, I., Salditt, T., & Safinya, C.R. Structure of DNA-Cationic liposome complexes: DNA Intercalation in multilamellar membranes in distinct interhelical packing regimes. Science. 1997, 275, 810–814.
[130] Izumitani, Y. Cation dipole interaction in the lamellar structure of DPPC bilayers. J. Colloid and Interface Sci. 1994, 166, 143–159.
[131] Pabst, G., Hodzic, A., Štrancar, J., Danner, S., Rappolt, M., & Laggner, P. Rigidification of neutral lipid bilayers in the presence of salts. Biophys. J. 2007, 93, 2688–2696.
[132] Uhríková, D., Pullmannová, P., Bastos, M., Funari, S.S., & Teixeira, J. Interaction of short-fragmented DNA with dipalmitoylphosphatidylcholine bilayers in presence of zinc. Gen. Physiol Biophys. 2009,28, 146–159.
[133] May, S., Harries, D., & Ben Shaul, A. The phase behavior of cationic lipid-DNA complexes. Biophys. J. 2000, 78, 1681–1697.
[134] Harries, D., May, S., Gelbart, W.M., & Ben Shaul, A. Structure, stability, and thermodynamics of lamellar DNA-lipid complexes. Biophys. J. 1998, 75, 159–173.
[135] Mengistu, D.H., Bohinc, K., & May, S. Binding of DNA to zwitterionic lipid layers mediated by divalent cations. J. Phys. Chem. B. 2009, 113, 12277–12282.
[136] Wagner, K., Harries, D., May, S., Kahl, V., Radler, J.O., & Ben Shaul, A. Direct evidence for counterion release upon cationic lipid-DNA condensation. Langmuir. 2000, 16, 303–306.
[137] Ruocco, M.J., & Shipley, G.G. Characterization of the sub-transition of hydrated dipalmitoylphosphatidylcholine bilayers – kinetic, hydration and structural study. Biochim. Biophys. Acta. 1982, 691, 309–320.
[138] Petrache, H.I., Tristram-Nagle, S., & Nagle, J.F. Fluid phase structure of EPC and DMPC bilayers. Chem. Phys. Lipids. 1998, 95, 83–94.
[139] Lengyel, A. Interakcia DNA s fosfolipidovými lipozómami v prítomnosti dvojmocných katiónov. / DNA interaction with phospholipid bilayer in presence of divalent cations. [PhD thesis]. Faculty of Pharmacy: Comenius University in Bratislava; 2010, 137–142.
[140] Koynova, R., & Caffrey, M. Phases and phase transitions of the phosphatidylcholines. Biochim. Biophys. Acta. 1998, 1376, 91–45.